HHS Public Access

Author manuscript

Biomaterials. Author manuscript; available in PMC 2017 August 20.

Published in final edited form as:

Biomaterials. 2017 January ; 113: 279–292. doi:10.1016/j.biomaterials.2016.10.054.

Neuroadhesive L1 coating attenuates acute microglial attachment to neural electrodes as revealed by live two-photon microscopy

James R. Eles[a,b], **Alberto L. Vazquez**[a,e,f], **Noah R. Snyder**[a,b], **Carl Lagenaur**[f], **Matthew C. Murphy**[e], **Takashi D.Y. Kozai**[a,b,c,d,**,1], and **X. Tracy Cui**[a,b,c,*,1]

[a]Bioengineering, University of Pittsburgh, United States

[b]Center for the Neural Basis of Cognition, University of Pittsburgh and Carnegie Mellon University, United States

[c]McGowan Institute for Regenerative Medicine, University of Pittsburgh, United States

[d]NeuroTech Center of the University of Pittsburgh Brain Institute, United States

[e]Radiology, University of Pittsburgh, United States

[f]Neurobiology, University of Pittsburgh, United States

Abstract

Implantable neural electrode technologies for chronic neural recordings can restore functional control to paralysis and limb loss victims through brain-machine interfaces. These probes, however, have high failure rates partly due to the biological responses to the probe which generate an inflammatory scar and subsequent neuronal cell death. L1 is a neuronal specific cell adhesion molecule and has been shown to minimize glial scar formation and promote electrode-neuron integration when covalently attached to the surface of neural probes. In this work, the acute microglial response to L1-coated neural probes was evaluated *in vivo* by implanting coated devices into the cortex of mice with fluorescently labeled microglia, and tracking microglial dynamics with multi-photon microscopy for the ensuing 6 h in order to understand L1's cellular mechanisms of action. Microglia became activated immediately after implantation, extending processes towards both L1-coated and uncoated control probes at similar velocities. After the processes made contact with the probes, microglial processes expanded to cover 47.7% of the control probes' surfaces. For L1-coated probes, however, there was a statistically significant 83% reduction in microglial surface coverage. This effect was sustained through the experiment. At 6 h post-implant, the radius of microglia activation was reduced for the L1 probes by 20%, shifting from 130.0 to 103.5 μm with the coating. Microglia as far as 270 μm from the implant site displayed significantly lower morphological characteristics of activation for the L1 group. These

*Corresponding author. Department of Bioengineering, University of Pittsburgh, 5057 Biomedical Science Tower 3, 3501 Fifth Avenue, Pittsburgh, PA, 15260, United States, xic11@pitt.edu (X.T. Cui). **Corresponding author. Department of Bioengineering, University of Pittsburgh, 208 Center for Bioengineering, 300 Technology Dr., Pittsburgh, PA, 15219, United States., tdk18@pitt.edu (T.D.Y. Kozai).

[1]Equal contribution.

Appendix A. Supplementary data

Supplementary data related to this article can be found at http://dx.doi.org/10.1016/j.biomaterials.2016.10.054.

results suggest that the L1 surface treatment works in an acute setting by microglial mediated mechanisms.

Keywords

Surface modification; Protein immobilization; Biomimetic coatings; Neural camouflage; Foreign body response; Microelectrode implants

1. Introduction

Chronically implanted neural electrodes have emerged as basic neuroscience research tools and effective therapeutics [1–6]. Specifically, microscale recording and stimulation electrodes have played a fundamental role in understanding and modulating the basic neural circuitry underlying complex neural networks [7–11] . In human clinical applications, implantable brain computer interface devices have demonstrated great promise in the ability to restore functional motor control [12,13]. However, the recording potential of implanted neural electrodes is limited by instability since the signal quality degrades over months to years post implant [7,14–17] . The degradation of the signal quality over time is understood to be a combination of material failure and biological factors [18].

Material failures largely result from corrosion and delamination of the electrode sites [19–25], cracks in the electrical traces [26–28], and delamination of insulation materials [18,25,28–30], all of which are exacerbated by perpetual strain caused by tissue micromotion during movement [28,31,32]. Biological failure modes of neural interfaces result from multiple sources that ultimately lead to meningeal cell invasion and fibrous encapsulation [14,33], insulting glial scar encapsulation, and neural degeneration [34,35]. Electrode insertion is a traumatic process, and even insertions that avoid large pial arteries and veins will break capillaries in the cortex, causing blood-brain barrier disruption [18,36,37]. This leads to an influx of plasma proteins that adsorb onto the surface of microelectrodes [18,36] and infiltration of inflammatory cells [38–40]. The combination of plasma proteins and cells, necrotic cell debris, and mechanical strain imposed by probe insertion causes an upregulation of proinflammatory cytokines that initiate the cascade of reactive tissue response [18,41–44]. Using two-photon microscopy, we have observed that nearby resident microglia immediately activate by retracting most of their processes while extending a few processes towards the probe in order to cover the surface of the implant with a lamellipodia sheath [41]. Over the following days, microglia and astrocytes aggregate at the surface of the implant to form an electrically insulating astroglial sheath [35,38,39,45,46]. Additionally, chronic inflammation leads to neural degeneration which presumably diminishes signal [18,24,42]. Lastly, failure is also fueled by the decrease in metabolic supply and neurotoxic waste product removal from loss of blood flow perfusion and increased metabolic consumption from inflammation [18,41,42].

In order to improve neural interface performance longevity, neural engineers have explored numerous intervention strategies. This includes changing the footprint of the probe or the probe’s electrode sites [18,36,44,47–51,160], altering recording site materials [48,52–57], applying flexible geometries or soft materials [26,27,36,58–62,161,162], creating

dissolvable insertion shuttles for softer probe materials [63], locally delivering anti-inflammatory or neuroprotective drugs [64–75], and modifying the probe's surface chemistry [36,76–78].

One promising method involves covalently attaching L1 cell adhesion molecule (L1) to the surface of the probe. L1 is a transmembrane cell surface glycoprotein that functions through homophilic interactions with L1 molecules on other cells to mediate cell recognition and cell interactions [79,80]. It has been shown to play a critical role in neuronal adhesion, axonal growth, neural migration, neural differentiation, and neuronal survival [81–89]. L1 is also implicated in improving regeneration following lesions in both the central and peripheral nervous systems [90–97]. Several studies have shown that L1 promotes neuronal cell attachment and growth while inhibiting glial and fibroblast cell attachment *in vitro* [98–101]. In the context of neural implants, our group has shown that covalent attachment of brain tissue derived L1 to neural probes can reduce glial scarring, while simultaneously encouraging neuronal attachment to the probe's surface for at least 2 months post-implant [61,76,77]. While these studies suggest L1 can modify the behavior of glial scars, the mechanism behind this is unclear. In the present work, we use two-photon microscopy (TPM) to study the dynamic microglial response to L1 coated microelectrodes for the first 6 h post-implant in living mice, as the first step to uncover the mechanisms. Compared to uncoated microelectrodes, there was significantly less microglial coverage of the L1 probes from 8 min–6 h post-implant, despite similar degrees of microglial process extension toward both coated and control probes. This suggests that L1's mechanism for preventing glial attachment and scarring occurs rapidly after initial contact.

2. Methods

2.1. Neural probes and L1 protein immobilization

All studies were performed using four-shank NeuroNexus 16-channel, 15 μm thick, 3 mm long SOI silicon probes (NeuroNexus Technologies, Ann Arbor, MI) mounted on dummy boards.

For quantitative analysis, L1 immobilization was conducted along the entire shank of the probes (n = 7), and all control probes (n = 7) were pristine, uncoated arrays that were washed with ethanol and phosphate buffer solution. L1 immobilization on the silicon dioxide surface and iridium oxide electrode pads were carried out as previously described with minor modifications [77,99]. Briefly, probes were cleaned and functionalized with either HNO3 (Sigma Aldrich) or by serial washes in acetone, 50% (v/v) MeOH/ H2O, and chloroform before oxygen plasma cleaning (30W) for 1 min (Harrick Plasma, PDC-001) [102]. Probes were silanized by immersion in 2% (3-mercaptopropyl) trimethoxysilane (Sigma Aldrich) solution with 4-maleimidobutyric acid N-hydroxysuccinimide ester (2 mM, Sigma Aldrich) for 1 h. Finally, probes were fully immersed in a 100 (μg/ml solution of purified L1 protein (purified at our lab) for 1 h at 4 °C, and stored in sterile 1 × phosphate buffer solution (Sigma Aldrich) until implantation. In an additional validation experiment (n = 1), following silanization of the probe's full surface, the probe was dipped only ~150 μm in the L1 solution. This half-coating design allowed for comparison between L1 and no L1 conditions on the same probe (Supplemental Fig. 1). The L1 modified probes were stored in

saline for up to 1 h prior to implantation. Previous studies have shown that the L1 coating procedure yields a uniform 6.37 nm thick coating with 0.53 g cm^{-3} density and increased hydrophobicity (water contact angle: 69.8 ± 1.7° for L1 coated v. 27.3 ± 1.4° for unmodified control) [99].

2.2. Surgery and probe insertion

Surgical procedures were conducted as previously described with 14 adult CX3CR1-GFP transgenic mice with GFP expression in macrophages and microglia controlled by the CX3CR1 promotor (Jackson Laboratories, Bar Harbor, ME) [41]. A cocktail of intraperitoneally (IP) administered ketamine/xylazine (90/8 mg kg^{-1}) was used to induce anesthesia, with depth of anesthesia assessed by monitoring the toe-pinch response, breathing, and heart rate. After animals were secured in a stereotaxic frame, scalps were shaved, cleaned with 70% ethanol, and resected. Calvarial periosteum was scraped off with cotton swabs, and a thin layer of Vetbond (3 M) was applied to dry the skull. A 1–1.5 mm tall well of light-curable cement (Composite Flowable; Henry Schein, NY, USA) was set around the margin of the exposed skull, following which a ~4–6 mm craniotomy was performed with a high-speed dental drill over the visual cortex (V1 and V2; centered approximately 2–3.5 mm caudal to Bregma and 1–3 mm lateral from midline). The craniotomy site was frequently washed with saline to remove bone fragments and prevent thermal damage of the underlying brain. A dental cement well was cured around the margin of the craniotomy to hold a saline immersion with the microscope objective. After the skull was thinned, it was carefully removed with fine-tip forceps. Following craniotomy, animals were placed under a two-photon microscope using a 16x, 0.8 numerical aperture water immersion objective (Nikon Inc., Milville, NY). Probes were stereotaxically targeted within the V1/V2 portion of the craniotomy and inserted in a rostral direction into the cortex at a 30–35° angle and parallel to midline at 50–100 μm s^{-1} (oil hydraulic microdrive; MO-81, Narishige, Japan) to a final resting depth of 250–300 μm (layer II–III) beneath the surface of the brain (Fig. 1). Major blood vessels were identified prior to insertion and avoided. All animals had a similar density of capillaries within the imaging window. Little or no bleeding was observed during insertion, though some spontaneous bleeding was observed throughout the 6 h experiment. Immediately prior to imaging, sulforhodamine 101 (SR101) was injected IP as a vascular contrast agent (red; 0.02–0.04 cc; 1 mg ml^{-1}). Updates of SR101 (0.01 mg ml^{-1}) and ketamine (22.5 mg kg^{-1}) were administered approximately every 30 min to maintain vascular contrast and a deep anesthetic plane. Updates of ketamine and SR101 were given through an IP catheter line (Braintree Scientific, Inc., USA). Minimal edema was observed throughout the 6 h experiment. All procedures and experimental protocols were approved by the University of Pittsburgh, Division of Laboratory Animal Resources and Institutional Animal Care and Use Committee in accordance with the standards for humane animal care as set by the Animal Welfare Act and the National Institutes of Health Guide for the Care and Use of Laboratory Animals.

2.3. Two-photon imaging

In vivo imaging was conducted with a two-photon laser scanning microscope consisting of a scan head (Prairie Technologies, Madison, WI), a Ti:sapphire laser (Mai Tai DS; Spectra-Physics, Menlo Park, CA) tuned at a wavelength of 920 nm, and non-descanned

photomultiplier tubes (Hamamatsu Photonics KK, Hamamatsu, Shizuoka, Japan) in whole-field detection mode to collect emitted light. Images were collected on Prairie View software. *ZT* stack images were collected every minute from 1 min prior to 79 min after probe insertion, and then *Z*-stack images at 80 min post-implant and every hour from 2 to 6 h post-implant were collected. Sterile saline was held in the craniotomy site by a dental cement well. This allowed for brain hydration and adequate water immersion for the microscope objective. Saline was replenished as it evaporated.

Both the initial *ZT*-stack images and hourly *Z*-stack images covered an area of 407.5 to 407.5 μm (1024 × 1024 pixels) at a scan rate of ~4.8 s/image, which gave sufficient resolution to track individual microglial processes. This image size allowed us to visualize 2–3 shanks at a time. Prior to probe insertion, continuous collection of 24 μm thick *ZT*-stacks (2 μm intervals between images; parameters set to maximize data collection at 1 min intervals) focused on the lowest depths of the intended insertion site commenced. Following the first *Z*-stack scan, probes were inserted and *ZT*-stack collection continued through the first 79 min post implant. Following initial *ZT*-stack collection, *Z*-stacks capturing the full observable depth of the implanted cortex were taken at 80 min post-implant and every hour from 2 to 6 h post-implant.

2.4. Data and statistical analysis

For each animal, *ZT*-stack images were analyzed to track individual microglial process positions over time and microglial surface coverage of the neural probes over time. Images with observable motion or drift from normal breathing, heartbeat, or tissue relaxation were corrected with a custom-written MATLAB script (Math Works, Boston, MA) using a rigid-body translation algorithm based on cross-correlation as previously described [41]. Alternatively, the “StackReg” plugin for ImageJ was used for rigid-body corrections of large motions [103]. Animals or microglial processes were discounted for any time-points in which motion could not be corrected or if there was poor visibility due to dural bleeding. Microglia process migration toward the probe tracked by recording XY coordinates of processes using the ‘Measure’ function in ImageJ (National Institutes of Health). The determination of migration toward the probe or away from the probe was systemized by dividing each microglial cell body into a hemisphere facing the probe and a hemisphere facing away from the probe. The line between hemispheres was defined as the line parallel to the nearest probe edge and that went through the midpoint of microglial cell body (examples of line selection shown in Fig. 6B). In order to negate any artefactual migration due tissue displacement upon probe insertion, measurements began after the probe’s entry. Time series movies were created with respect to the time stamps of individual frames. Microglial surface coverage of the probe and percent of tissue with microglial signal was determined by making a binary mask of a sum projection of each *ZT*-stack using the ImageJ Default variant of the IsoData threshold method [104]. An outline of the probe was manually defined by focusing on planes below the surface of the probe, where the profile of the probe appeared as dark shadow with high contrast between the edge of the probe and the fluorescence of the parenchyma. The dimensions of the probe outline were cross referenced with the dimensions of the device to ensure accuracy. Because there is likely disproportionate strain in tissue surrounding the tip of the probe due to micromotion, the

first 30 μm of the probe from the tip was discounted from analyses [105]. Non-zero pixels were counted using the 'Measure' function, and divided by the area of the user-defined probe outline to derive the % surface coverage of the probe by microglial and the percent of tissue with microglial signal.

Z-stacks of the full observable depth of implanted cortex at 80 min and 2–6 h post-implant were analyzed to determine the extent of microglial surface coverage of the probe and the morphology of microglia surrounding the implant. For the quantification of microglial coverage of the probe, the *Z*-stacks were first digitally rotated 25–35° with Interactive Stack Rotation plugin for ImageJ in order to view the surface of the entire probe in one rotated *Z* plane [106]. The sum of *Z*-stack comprising the surface of the probe and the 20 μm above the probe were projected onto one image. Microglial surface coverage was then measured as described above.

For qualitative evaluation of the microglial reaction, *Z*-stacks were transformed from XY planes to XZ or YZ planes by linear interpolation (ImageJ; '3D Project' function). Average intensity or sum projections of reconstructed stacks allowed for analysis of specific regions of interest.

Changes in process velocity and microglial surface coverage of the probe with respect to time and changes in percent of tissue with microglial signal with respect to distance were modeled using a linear mixed effects model with random slopes and intercepts for each animal. To allow the model to fit nonlinear relationships, a restricted cubic spline basis was implemented with 4 knots placed at the 5th, 35th, 65th, and 95th percentiles of the data. Additional fixed effects included a categorical variable for group (L1 versus control) and the interaction between group and time. To test for any significant group-wise differences a likelihood ratio test was performed comparing two models: (1) the full model described above; and (2) a second model that excluded the group and group-by-time interaction predictors. Confidence intervals were estimated using case bootstrapping with 1000 iterations. 95% confidence intervals were computed as 1.96 times the standard error of the model fits.

The 6 h post-implant *Z*-stacks were used to characterize microglia morphology. Microglia were classified as ramified (1) if processes extended in all directions without preference, or in the activated transitional stage (T-stage) (0) if processes were selectively extended toward the implant insertion site (Fig. 1C) [21]. The determination of the direction that was toward the insertion site was made by the same hemispheric distinction described in the microglial velocity analysis description above. Microglia were binned by distance from the probe. From these values, a logistic regression was created to show the Bernolli Probability Distribution of microglia being in the ramified state (0 or 1) as a function of distance from the probe. Because probability distribution inherently accounts for error, there can be no additional calculation of error for this data.

Morphology was also used to assess the degree of microglial activation through a transitional stage morphology index (T-index) and a microglia directionality stage index (D-Index). The T-Index was calculated by measuring the length of the longest microglia process

facing the probe (*n*) and the length of the longest process facing away from the probe (*f*). The D-Index was calculated by measuring the number of microglial processes projecting toward the probe (*n*) and away from the probe (*f*). *n* and f were then used to calculate respective index values through the following formula:

$$\text{Index}=\frac{(f-n)}{(f+n)}+1 \quad (1)$$

For both indices, a value of 1 (*n* = *f*) indicates that a microglia extends processes in all directions without preference (ramified morphology). Index values < 1 indicate a preference in either process length (T-Index) or process number (D-Index) in the direction of the probe. Cells were binned by 30 μm distance intervals from the probe, which was selected to insure at least 10 samples per interval. To determine how microglial activation varied with distance from the probe, data was fitted to a custom MATLAB dual sigmoidal function. This model was previously optimized in studies of acute microglial reaction to different neural implants, and therefore allows for comparison between studies [41,75]. The model has parameters for amplitude (*a*), shoulder location (d_1 and d_2; μm), and shoulder width (w_1 and w_2; μm):

$$y(d)=\frac{a}{1+e^{(d-d_1)/w_1}}+\frac{1-a}{1+e^{(d-d_2)/w_2}} \quad (2)$$

3. Results

In order to characterize the dynamic interactions of microglia with L1-coated neural probes in the first 6 h post-implantation, 7 probes with L1 protein immobilized along the full extent of all shanks and 7 pristine, uncoated control probes were implanted into the cortex of 14 CX3CR1-GFP reporter mice. Microglial dynamics were tracked in relation to the implanted probe with two-photon microscopy (TPM).

3.1. Microglia process extension velocity is unaffected by the L1 coating

Following craniotomy and vascular dye injection, we examined the surface of the brain with fluorescence microscopy for regions with low vascular density that would be suitable for imaging. Once a region was selected, we confirmed that there was no pre-existing microglial activation with TPM, and inserted the probe. For both the control probes and L1 coated probe, microglial processes ~175 μm from the probe extended toward the implant site immediately after insertion (Supplementary Movie 1 and 2). In order to quantitatively compare process extension between groups, the velocities of individual microglia process end-feet (total processes varied between 12 and 21 depending on time-point with 5 animals for each group; 2 animals from each group were discounted due to movement artifacts) were tracked from 4 to 79 min post-implant (Fig. 2A and B; representative movies of microglial reaction from 1 min prior to implant to 79 min post-implant shown in Supplemental Movie 1 and 2). Both control and L1 group microglia processes moved fastest within the first 30 min post-implant (between 0.5 and 1.5 μm/min), and slowed to a near-stop by the first 60 min post-implant, largely due to processes reaching the surface of the implant. There were no

significant group-wise differences in velocity between the control and L1 groups in the likelihood ratio test. Additionally, there was no statistical difference in aggregate microglia process movement toward and away from the probe between 4 and 79 min post-implant velocity between the L1 and control groups (Fig. 2C).

Supplementary video related to this article can be found at http://dx.doi.org/10.1016/j.biomaterials.2016.10.054.

3.2. Immediate and sustained inhibition of microglial surface coverage of the probe with the L1 coating

Once processes reached the edge or the face of the probe, the processes stopped migrating. However, once the process end-feet reached their destination, the microglia began covering the surface of the probe with lamellipodium sheaths. In order to characterize this microglial surface coverage, a threshold-based method was used to quantify the percent of the probe's face that was covered by processes between 4 and 79 min post-implant (Fig. 3; n = 4 per group; 3 were discounted from each group due to movement artifacts or lack of visual clarity due to bleeding). There were significant group-wise-differences between the control and L1 coated probes (Likelihood ratio test, $p < 0.01$), with the 95% confidence intervals of groups diverging by 8 min post-implant, and remaining distinct for the remainder of the experiment. The face of L1 coated probes was less than 11% covered by microglia for the first 79 min post-implant. Coverage of control probes continued to increase, plateauing at 40–45% coverage by 30 min post-implant, and remaining statistically increased relative to L1 coated probes through the 79 min of imaging.

This effect of L1 coating preventing microglial surface coverage extended for hours (Fig. 4). At both 2 h and 6 h post implant, there was significantly less microglial surface coverage of L1 coated probes compared to control probes (2 h: 8.2± 2.4% v. 47.7± 3.4%, $p < 0.001$; 6 h: 6.2± 2.4% v. 35.8± 6.9%, $p < 0.05$; both comparisons by Welch's t-tests). There was no statistical difference within the same coating groups between 2 and 6 h post-implant. This effect was qualitatively corroborated by a validation experiment (n = 1) in which the first ~150 μm from the tip of the probe was coated with L1, leaving the rest of the probe uncoated (Supplemental Fig. 1). At 3 h post-implant, there was an observable reduction in microglial surface coverage of the L1-coated portion of the probe.

In order to determine how the amount microglial signal changed with Z-direction distance from the implant, thresholded side-projection images of 2 h post-implant *Z*-stacks were rendered. Looking at the % of tissue with microglial signal after thresholding, there were significant group-wise differences between L1 and control probes (Fig. 5; n = 3 per group, reduced due to availability of sufficiently sized *Z* stacks; Likelihood ratio test, $p < 0.0001$). In particular, there was a deviation in 95% confidence intervals of groups within the first 20 μm of the probe surfaces, with a 92–57% reduction in microglial signal between 0 and 20 μm above the L1 coated probes (Fig. 5B). Between 20 and 50 μm, however, the 95% confidence intervals converged for the groups, indicating that there was a similar amount of microglial signal in this region.

3.3. Changes in microglia activation at 6 h with L1 coating

At 6 h post-implant, there were several differences in microglia morphology between control and L1 groups. Microglia morphology was evaluated (n = 216 microglia for the control group; 253 microglia for L1 group, each from 5 animals) and classified as either ramified (1) or transitional stage (T-stage; 0) (Fig. 1C), and plotted average values against distance from the probe's edge (Fig. 6A and B). Logistic regression was then used to model the data:

$$\text{Control}: \log(p/1-p) = -7.63x + 0.059 \quad (3)$$

$$\text{L1}: \log(p/1-p) = -5.06x + 0.049 \quad (4)$$

where p denotes the probability that a microglia at a given radius (x) is ramified. The distance from the probe at which 50% of microglia were ramified was determined to be 130.0 μm for the control group and 103.5 μm for the L1 group.

In order to explore differences in the degree of microglial activation between the control and L1 groups, two morphology indices were evaluated: 1) a T-stage morphology index (T-Index), which compares the length of the longest process extending toward the probe vs. the longest process extending away from the probe for each microglia, and 2) a directionality index (D-Index), which compares the number of processes facing toward the probe vs. the number of processes facing away from the probe for each microglia. For both indices, values closer to 0 indicate a stronger response toward the probe, whereas an index value of 1 indicates either ramified or no preferential response toward the probe. Two-shouldered sigmoidal functions were fit to the data of both indices using Equation (2) with parameters for relative amplitude (a), near shoulder (d1) and spread (w1), and far shoulder (d2) and spread (w2). For the T-index, control parameters were a—0.65, d1—10.35 μm, w1—21.04 μm, d2—215.11 μm, and w2—5.00 μm, and L1 parameters were a—0.85, d1—58.63 μm, w1—23.94 μm, d2—146.25 μm, and w2—5.00 μm (Fig. 6C). Comparing general trends of sigmoidal curves of the control and L1 group T-Indices, both groups had very low index values immediately adjacent to the probe, with few microglial processes protruding far away from the implantation site. Interestingly, the microglia between 30 and 60 μm from the L1 coated probes had a significantly lower T-index value compared to microglia around the control probes (Welch's T-test; $p < 0.001$). As noted in our previously published work, microglia between 60 and 210 μm from the control probes held at a 0.6 T-index. Contrary to this, microglia in the same region around L1 coated probes had progressively increasing T-index values, reaching a value of ~1 by 150 μm from the probe. Microglia around control probes did not reach a "1" T-index value until 210 μm from the implant. This difference in T-index was reflected in T-tests, where the L1 group had statistically higher T-index values between 150–210 and 240–270 μm from the probe (Welch's T-test; $p < 0.05$).

There were also differences between the control and L1 group in the D-Index values (Fig. 6D). The sigmoidal function parameters for the control were a—0.79, d1—10.54 μm, w1—15.45 μm, d2—186.03 μm, and w2—25.06, and for the L1 group were a—0.82, d1—43.45

μm, w1—14.54 μm, d2—141.28 μm, and w2—9.65 μm. Microglia within 60 μm of L1 coated probes had significantly lower D-Index values when compared to microglia around control probes (Welch's T-Test; $p < 0.05$). Beyond 60 μm, D-Index values continued to rise without any significant differences between groups, reaching a "1" D-index value around 180 μm from the probe. The D-Index for the L1 group was significantly higher than the control group between 270 and 300 μm (Welch's T-test; $p < 0.05$).

4. Discussion

The value of implantable microelectrode technologies as basic-research tools and substrates for brain-machine interfaces is well established, however, their clinical implementation has been stifled by their high failure rate in pre-clinical models. Covalently linking neural adhesion molecule L1 to the neural probe's surface is a promising strategy to improve biocompatibility. *In vitro*, substrate-bound L1 can selectively encourage neuronal attachment while deterring astrocyte and fibroblast attachment [98,99,101]. *In vivo*, we have previously shown that L1 coatings on probes implanted in the cortex, spinal cord, and dorsal root ganglia improve neuronal survivability, axonal regeneration, and even neuronal attachment to probe's surface for at least 8 weeks post-implant [61,76,77]. This is distinct from other coating strategies (laminin, Parylene-C, PDMS, PEG/polyurethane) which may attenuate some neuronal cell death, but do not improve regeneration [107–109]. Further, the microglial and astrocytic responses are attenuated in the region immediately surrounding the probe. These results were obtained via postmortem histology at discrete chronic time-points, while the specific interaction between the L1 coating and the host cells that leads to these effects remains unclear. Towards this end, the current experiment assessed the acute microglial response to L1-coated substrates in cortex immediately after implantation, providing mechanistic clues to describe L1's therapeutic effects.

4.1. Microglial process extension and probe surface coverage

As in our previous work, within 5min after implantation of L1 or control probes, most microglia within 100 μm became polarized, extending processes toward the implantation site while retracting processes that were initially facing away from the probe [41]. Polarization and process extension indicate microglia activation, and are often followed by cell body movement toward the source of activation (12 + hours to days) [38,39,110–112] . These processes extended until they reached the edge or surface of the probe, approximately 30–45 min post-implant, dependent upon the initial position of the process. There were no significant differences in the process extension velocities between the groups. This suggests that process extension is mediated by factors that are independent of the covalently attached L1 surface coating. The most likely factors are soluble chemokines or debris released from damaged cells, mechanically stimulated release of soluble chemokines, and blood plasma proteins release from the mechanically damaged BBB. Chemokines such ATP, UDP, and glutamate are known to incite directed microglial process extension along the chemokine gradient [113–117] . Upon mechanical trauma, astrocytes and neurons release ATP and glutamate into the extracellular space, serving as chemokines for surrounding microglia [118–120]. This effect is conserved across many paradigms of mechanical trauma, including deep-brain stimulator implantation in humans [121]. It is not known if abrupt mechanical

distortions directly affect microglial phenotype, though recent studies have shown that microglial behavior is modulated by at least some mechanical cues. Namely, if placed on a substrate with a gradient of stiffness, cultured microglia will migrate toward the stiffer areas [122].

In addition to mechanically stimulated release of chemokines, probe implantation will also mechanically rupture blood vessels, causing release of blood plasma proteins such as immunoglobulins, serine proteases, and albumin into injury site [37]. Diffusing through cortex at ~137 μm min^{-1}, these proteins—which are known to perpetuate microglial responses and contribute to neuronal death—will have spread through the volume of the entire viewing area of this study within the first 5 min post-implant [123–128]. These plasma proteins can also physically adsorb to the surface of the probe, which may have an effect on the phenotype of cells that contact the probe's surface [36,99].

Most processes stopped extension once they reached the surface of the probe. The percent of the probe's surface that was covered in these processes increased over the 6 h experiment for both groups. There was, however, significantly less coverage of the L1 probes as early as 8 min post-implant. At all points between 8 min and 6 h post-implant, there was a 75–83% reduction in surface coverage of the L1 group. There was a slight drop in surface coverage between 2 and 6 h post-implant for both the L1 and control groups, but it is not clear if that is due to microglial process retraction, or dimming of the image quality due to spontaneous bleeding or gradual photobleaching. However, the drop was not statistically significant, and the reduction in surface coverage was the same (83%) at both 2 and 6 h post-implant. We postulated that there were two possible mechanisms to explain the reduction in microglial surface coverage of the L1 group: the endfeet that were contacting or immediately adjacent to the L1 probe were smaller and covered a smaller area of the probe, or activated, T-stage microglia were projecting fewer professes to the surface of the L1 probe. To investigate these possibilities, we examined how the amount of microglial signal changed with distance from the probe's surface. If the first possibility was true, we would expect that the decrease in microglial signal for L1 probes would be confined to the region immediately adjacent to the surface of the probe, and there would be no difference between groups further away from the probe. In the second scenario, there would be fewer processes and therefore less microglial signal for the L1 group throughout the radius of microglial activation (<17 5 μm from probe, as seen in Fig. 6a). Our evidence points to the former—there were a similar number of microglial processes directed toward both types of probes, but within 20 μm of the L1 probe, there was a decrease in microglial signal. This suggests that L1's effect modulated the endfeet and processes contacting or immediately adjacent to the coating. Qualitative observations of the microglial surface coverage tissue corroborate this mechanisms, in which coverage tissue often appeared as flattened, contiguous swathes of tissue on control probes, but easily discernable 1–2 μm diameter endfeet on L1 probes (Fig. 3a).

While it is likely that microglial processes are guided to the probe along a chemotactic gradient generated by implantation trauma, it is unclear why microglial processes attach to the surface of the probe. It is believed that microglia make prolonged contacts with injury sites to uptake neurotoxic or excitotoxic factors released from damaged cells or vasculature

[129–131], reconstitute damaged barriers between the brain and the rest of the body [113,132], and phagocytose damaged neurons, plaques, or invading neutrophils [133–135]. One possibility is that these inflammatory factors adsorb onto the surface of uncoated electrodes leading to prolonged microglial contact [36]. It is unclear how L1 is influencing these particular microglial functions. For NCAM, terminal sialic acid residues can suppress microglial phagocytosis through the SIGLEC-E receptor [133]. Though it has not been tested, it is possible the sialic acid residues on L1 could act similarly. Further, it is unclear how this surface coverage behavior would affect the longevity and long-term outcome for the implanted device.

4.2. Possible mechanisms of the L1-coating effect

Taken together, the process extension data and surface coverage data suggest that the L1 did not have an effect on the microglia until after they made physical contact with the coating or were within 25 μm of the probe's surface. Interestingly, while many cells of hematopoietic origin express L1, to our knowledge microglia do not, and so cannot engage in the L1-L1 homophilic binding that neurons exploit [136]. L1, however, is known to make heterophilic interactions with the proteoglycans phosphacan and neurocan as well as the integrins α5β3 in humans and rodents and α5β1 in mice [137–139]. Of these potential heterophilic binding sites, microglia at least express α5β1, and expression increases upon cytokine activation [140–142]. While there are no specific studies on the interaction between microglial α5β1 and L1, this could be a potential mechanism by which the L1 coating is attenuating microglial surface coverage behavior. Further, as described above, it is possible that L1's terminal polysialic acid residues could bind to the microglial SIGLEC-E receptor, which suppresses phagocytosis.

In support of direct interaction between L1 and adjacent microglia is the observation that morphological differences exist between the two groups at 6 h post-implant. To understand the microglial morphology, cells were first defined as either ramified or T-stage by qualitative assessment, and then the number (D-Index) and length (T-Index) of individual processes that were projecting toward the probe were compared to processes that were projecting away from the probe. This allowed the characterization of trends in microglial activation as well as the degree of microglial activation. While the qualitative ramification index shows that there were more ramified microglia closer to the L1 implants, both the T-Index and D-Indexes were lower for the L1 group at points within 60 μm of the probe. This indicates that microglia within 60 μm of the L1 probes had more processes and longer processes extending toward the probe compared to microglia within 60 μm of the control probes. While this may suggest that the microglia in the immediate vicinity of the L1 probes are more "activated", the L1 probes had an 83% reduction in microglial surface coverage at this same time point. This data suggests that, while the microglia are more activated, the phenotype of activation is different. Many recent studies have suggested that there is a continuum of microglial activation states, often broadly stated in terms of M1, which is proinflammatory and can lead to scarring, or M2 activation, which is anti-inflammatory, and is important in phagocytosing cell debris and tissue regeneration [143–145]. While trauma such as a neural probe implantation may drive M1 microglia activation, perhaps interacting with the L1 coating alters the activation state of microglia [144]. *In vitro* studies are

conflicting as to whether M1 and M2 microglia have different morphologies [146] or not [147,148], and thus future studies looking at early time-point immunohistochemical markers for microglia polarization will be necessary to address this. Importantly, microglial activation could have consequences for neuronal health. Activated microglia have been implicated in directly causing or exacerbating phagocytotic, excitotoxic, and apoptotic neuronal death [34,35,149,150]. Interestingly, previous work has shown that tissue around L1 coated probes had both fewer activated microglia as well as an increase in neuronal processes after 8 weeks of implantation when compared to healthy tissue and uncoated probes [77]. This suggests that the L1 coating has a neuronal regeneration effect, unlike dexamethasone coatings, which can reduce microglial activation but don't lead to neuronal regeneration [70]. It is unclear whether this regenerative effect is due to L1's action on neurons, microglia, or both. Future experiments should be focused on isolating these effects to achieve a full understanding of L1's mechanisms.

The morphology index data also suggests that there is an indirect interaction between the L1 coating and microglia. At 6 h post-implant, the T-index for the L1 group was significantly higher at points between 150 and 270 μm and the D-Index was higher between 240 and 270 μm, areas with cells that had no direct contact with the probe. It is possible that cells contacting the L1 coating—either microglia, astrocytes, or neurons—are releasing molecules or changing expression of membrane proteins in such a way to affect the phenotype of cells in this distant region. Supporting this are *in vitro* and *in vivo* studies of peripheral macrophages show that surface chemistry can affect secreted cytokine profiles within 1 day of implant [151,152] The areas between 60 μm and the distant regions were not different between coating groups. This may indicate that this area was still affected by mechanical changes due to probe insertion or soluble factors from damaged cells and blood vessels. The distant region that had significant changes between groups may have been out of range of these mechanical and chemical changes, but still within the range of L1-related changes.

It is also possible that the difference in hydrophobicity between the control and the L1 probes affected the microglial response. In previous studies, we have shown that the water contact angle for the unmodified control and L1 coated probes are respectively 27.3 ± 1.4° and 69.8 ± 1.7° [99]. In these previous studies, however, we showed that L1 functionalized substrates had distinct effects on primary neuron and astrocyte adhesion when compared to L1-free substrates with similar hydrophobicity. Further, in an experiment with a probe that had a region of L1 functionalization and a region of silane + GMBS treatment, there was an observable reduction in microglial surface coverage for the L1 region when compared to the silane + GMBS side at 3 h post-implant (Supplemental Fig. 1). This corroborates that L1 has a distinct, bioactive effect when compared to a surface with comparable hydrophobicity (Water contact angle: L1: 69.8 ± 1.7°, silane + GMBS: 58.5 ± 1.6° [99]). Nevertheless, hydrophobicity of the surface is expected to play a role in protein adsorption and the consequent cellular interaction. A separate study is ongoing to examine the microglia response to well-controlled non-bioactive surfaces with different hydrophobicity.

4.3. Long-term effects of L1 coatings and future directions

While the present study shows that the L1 coating is effective in reducing microglial surface coverage through 6 h post-implant, our previous work shows that the L1 coating is effective in reducing glial scarring and neuronal cell death to at least 8 weeks post implant [61,76,77]. It is unclear how these initial effects on micro-glial dynamics transitions into the effects observed at late time points. Further, the present study demonstrates that while the L1 probes had less surface coverage, microglia around those probes had more morphological activation. Future studies will need to track these populations of activated microglia to study their long-term fate and role in glial scar formation. To address this, our group has also optimized cranial window techniques that enable longitudinal imaging from 12 h post-implant to at least 3 months post-implant [46].

While we have seen how microglia interact with the L1 coating, neurons, astrocytes, and oligodendrocytes also likely to interact with the coating [91,98,99,101,153,154]. Animal models with transgenic labels in multiple cell types—such as neurons with expression of the calcium indicator GCaMP—could be crucial in understanding the complex effects the coating is playing [155]. Current efforts are underway to follow this work with chronic imaging studies of the long-term microglial and neuronal responses to L1 probes including microglial cell body migration and aggregation at the tissue-probe interface as well as changes in neuron distribution and electrophysiology over time.

In addition to L1, other cell-surface proteins implicated in modulating microglia-neuron or neuron-neuron interactions could be used alone or in synergy with L1 as a neural probe coating [101,156–159]. Addressing these experiments will help to provide a framework for a broadly applicable bioactivity assay for novel neural technologies using longitudinal *in vivo* microscopy. Additionally, these experiments will improve our understanding of how surface modification affect the integration of foreign bodies into host tissue, which is crucial for implantable stimulation and recording probes as well as microdialysis probes, neurochemical sensors, drug delivery devices, and other types of neural implants [75].

5. Conclusion

The current study has demonstrated an immediate and substantial reduction of microglial surface coverage of neural probes with an L1 protein coating. This effect remained significant through 6 h post-implant (the duration of the experiment), corroborating previous findings that L1 coatings provide long-lasting mitigation of gliosis and neuronal cell death (at least 8 weeks). The coating reduced surface adhesion-behavior of microglia that were contacting the probe, and also reduced morphological activation of distant microglia that had no direct contact with the probes. This work provides both a framework for a rapid bioactivity assay for implantable neural technologies, as well as identifies microglia as a possible key mediator of the L1-coating’s long-lasting anti-gliosis effect. Ultimately, this study identifies novel pathways to improve the efficacy of implantable neural technologies and establishes two-photon microscopy techniques that can rapidly test and validate these novel pathways.

Supplementary Material

Refer to Web version on PubMed Central for supplementary material.

Acknowledgments

This project was financially supported by NIH NINDS (Grant 5R01NS062019, 1R01NS094396, 1R01NS089688). The authors would like to thank Patrick Cody, and Bin Cao for assistance with the coating procedures.

References

1. Kozai TDY, Vazquez AL. Photoelectric artefact from optogenetics and imaging on microelectrodes and bioelectronics: new challenges and opportunities. J. Mater. Chem. B. 2015; 3:4965–4978. http://dx.doi.org/10.1039/C5TB00108K.
2. Schwartz AB, Cui XT, Weber DJ, Moran DW. Brain-controlled interfaces: movement restoration with neural prosthetics. Neuron. 2006; 52:205–220. http://dx.doi.org/10.1016/j.neuron.2006.09.019. [PubMed: 17015237]
3. Schwartz AB. Cortical neural prosthetics. Annu. Rev. Neurosci. 2004; 27:487–507. http://dx.doi.org/10.1146/annurev.neuro.27.070203.144233. [PubMed: 15217341]
4. Kipke DR, Shain W, Buzsaki G, Fetz E, Henderson JM, Hetke JF, Schalk G. Advanced neurotechnologies for chronic neural interfaces: new horizons and clinical opportunities. J. Neurosci. 2008; 28:11830–11838. http://dx.doi.org/10.1523/JNEUROSCI.3879-08.2008. [PubMed: 19005048]
5. Cogan SF, Ludwig KA, Welle CG, Takmakov P. Tissue damage thresholds during therapeutic electrical stimulation. J. Neural Eng. 2016; 13:021001. http://dx.doi.org/10.1088/1741-2560/13/2/021001. [PubMed: 26792176]
6. Birmingham K, Gradinaru V, Anikeeva P, Grill WM, Pikov V, McLaughlin B, Pasricha P, Weber D, Ludwig K, Famm K. Bioelectronic medicines: a research roadmap. Nat. Rev. Drug Discov. 2014; 13:399–400. [PubMed: 24875080]
7. Kozai TDY, Du Z, Gugel ZV, Smith MA, Chase SM, Bodily LM, Caparosa EM, Friedlander RM, Cui XT. Comprehensive chronic laminar single-unit multi-unit and local field potential recording performance with planar single shank electrode arrays. J. Neurosci. Methods. 2015; 242:15–40. http://dx.doi.org/10.1016/jjneumeth.2014.12.010. [PubMed: 25542351]
8. Chestek CA, Gilja V, Blabe CH, Foster BL, V Shenoy K, Parvizi J, Henderson JM. Hand posture classification using electrocorticography signals in the gamma band over human sensorimotor brain areas. J. Neural Eng. 2013; 10:026002. http://dx.doi.org/10.1088/1741-2560/10/2/026002. [PubMed: 23369953]
9. Jia X, Smith MA, Kohn A. Stimulus selectivity and spatial coherence of gamma components of the local field potential. J. Neurosci. 2011; 31:9390–9403. http://dx.doi.org/10.1523/JNEUROSCI.0645-11.2011. [PubMed: 21697389]
10. Fraser GW, Chase SM, Whitford A, Schwartz AB. Control of a brain-computer interface without spike sorting. J. Neural Eng. 2009; 6:055004. http://dx.doi.org/10.1088/1741-2560/6/5/055004. [PubMed: 19721186]
11. Mizuseki K, Royer S, Diba K, Buzsáki G. Activity dynamics and behavioral correlates of CA3 and CA1 hippocampal pyramidal neurons. Hippocampus. 2012; 22:1659–1680. http://dx.doi.org/10.1002/hipo.22002. [PubMed: 22367959]
12. Collinger JL, Wodlinger B, Downey JE, Wang W, Tyler-Kabara EC, Weber DJ, McMorland AJ, Velliste M, Boninger ML, Schwartz AB. High-performance neuroprosthetic control by an individual with tetraplegia. Lancet. 2013; 381:557–564. http://dx.doi.org/10.1016/S0140-6736(12)61816-9. [PubMed: 23253623]
13. Hochberg LR, Bacher D, Jarosiewicz B, Masse NY, Simeral JD, Vogel J, Haddadin S, Liu J, Cash SS, van der Smagt P, Donoghue JP. Reach and grasp by people with tetraplegia using a neurally controlled robotic arm. Nature. 2012; 485:372–375. http://dx.doi.org/10.1038/nature11076. [PubMed: 22596161]

14. Barrese JC, Rao N, Paroo K, Triebwasser C, Vargas-Irwin C, Franquemont L, Donoghue JP. Failure mode analysis of silicon-based intracortical micro-electrode arrays in non-human primates. J. Neural Eng. 2013; 10:066014. http://dx.doi.org/10.1088/1741-2560/10/6/066014. [PubMed: 24216311]
15. Chestek CA, Gilja V, Nuyujukian P, Foster JD, Fan JM, Kaufman MT, Churchland MM, Rivera-Alvidrez Z, Cunningham JP, Ryu SI, V Shenoy K. Long-term stability of neural prosthetic control signals from silicon cortical arrays in rhesus macaque motor cortex. J. Neural Eng. 2011; 8:045005. http://dx.doi.org/10.1088/1741-2560/8/4/045005. [PubMed: 21775782]
16. Kipke DR, Vetter RJ, Williams JC, Hetke JF. Silicon-substrate intracortical microelectrode arrays for long-term recording of neuronal spike activity in cerebral cortex. IEEE Trans. Neural Syst. Rehabil. Eng. 2003; 11:151–155. http://dx.doi.org/10.1109/TNSRE.2003.814443. [PubMed: 12899260]
17. Williams JC, Rennaker RL, Kipke DR. Long-term neural recording characteristics of wire microelectrode arrays implanted in cerebral cortex. Brain Res. Protoc. 1999; 4:303–313. http://dx.doi.org/10.1016/S1385-299X(99)00034-3.
18. Kozai TDY, Jaquins-Gerstl AS, Vazquez AL, Michael AC, Cui XT. Brain tissue responses to neural implants impact signal sensitivity and intervention strategies. ACS Chem. Neurosci. 2015; 6:48–67. http://dx.doi.org/10.1021/cn500256e. [PubMed: 25546652]
19. Gilgunn, PJ., Ong, XC., Flesher, SN., Schwartz, AB., Gaunt, RA. Structural analysis of explanted microelectrode arrays; 2013 6th Int. IEEE/EMBS Conf. Neural Eng, IEEE. 2013. p. 719-722.http://dx.doi.org/10.1109/NER.2013.6696035
20. Luo X, Weaver CL, Zhou DD, Greenberg R, Cui XT. Highly stable carbon nanotube doped poly(3,4-ethylenedioxythiophene) for chronic neural stimulation. Biomaterials. 2011; 32:5551–5557. http://dx.doi.org/10.1016/j.biomaterials.2011.04.051. [PubMed: 21601278]
21. Cogan SF, Guzelian AA, Agnew WF, Yuen TG, McCreery DB. Over-pulsing degrades activated iridium oxide films used for intracortical neural stimulation. J. Neurosci. Methods. 2004; 137:141–150. http://dx.doi.org/10.1016/j.jneumeth.2004.02.019. [PubMed: 15262054]
22. McIntyre CC, Grill WM. Selective microstimulation of central nervous system neurons. Ann. Biomed. Eng. 2000; 28:219–233. [(Accessed 6 June 2016)] http://www.ncbi.nlm.nih.gov/pubmed/10784087. [PubMed: 10784087]
23. Jan E, Hendricks JL, Husaini V, Richardson-Burns SM, Sereno A, Martin DC, Kotov NA. Layered carbon nanotube-polyelectrolyte electrodes outperform traditional neural interface materials. Nano Lett. 2009; 9:4012–4018. http://dx.doi.org/10.1021/nl902187z. [PubMed: 19785391]
24. Kozai, TDY., Alba, NA., Zhang, H., Kotov, NA., Gaunt, RA., Cui, XT. Nanotechnol. Neurosci. Nano-electronic, Photonic Mech. Neuronal Interfacing. Springer New York; New York, NY: 2014. Nano-structured coatings for improved charge delivery to neurons; p. 71-134.http://dx.doi.org/10.1007/978-1-4899-8038-0_4
25. Prasad A, Xue Q-S, Dieme R, Sankar V, Mayrand RC, Nishida T, Streit WJ, Sanchez JC. Abiotic-biotic characterization of Pt/Ir microelectrode arrays in chronic implants. Front. Neuroeng. 2014; 7:2. http://dx.doi.org/10.3389/fneng.2014.00002. [PubMed: 24550823]
26. Ware T, Simon D, Liu C, Musa T, Vasudevan S, Sloan A, Keefer EW, Rennaker RL, Voit W. Thiol-ene/acrylate substrates for softening intra-cortical electrodes. J. Biomed. Mater. Res. B. Appl. Biomater. 2014; 102:1–11. http://dx.doi.org/10.1002/jbmb.32946. [PubMed: 23666562]
27. Lacour SP, Benmerah S, Tarte E, FitzGerald J, Serra J, McMahon S, Fawcett J, Graudejus O, Yu Z, Morrison B. Flexible and stretchable micro-electrodes for in vitro and in vivo neural interfaces. Med. Biol. Eng. Com-put. 2010; 48:945–954. http://dx.doi.org/10.1007/s11517-010-0644-8.
28. Kozai TDY, Catt K, Li X, Gugel ZV, Olafsson VT, Vazquez AL, Cui XT. Mechanical failure modes of chronically implanted planar silicon-based neural probes for laminar recording. Biomaterials. 2015; 37:25–39. http://dx.doi.org/10.1016/j.biomaterials.2014.10.040. [PubMed: 25453935]
29. Seymour JP, Elkasabi YM, Chen H-Y, Lahann J, Kipke DR. The insulation performance of reactive parylene films in implantable electronic devices. Biomaterials. 2009; 30:6158–6167. http://dx.doi.org/10.1016/j.biomaterials.2009.07.061. [PubMed: 19703712]

30. Kim, BJ., Washabaugh, EP., Meng, E. Annealing effects on flexible multi-layered parylene-based sensors; 2014 IEEE 27th Int. Conf. Micro Electro Mech. Syst, IEEE. 2014. p. 825-828.http://dx.doi.org/10.1109/MEMSYS.2014.6765768

31. Subbaroyan J, Martin DC, Kipke DR. A finite-element model of the mechanical effects of implantable microelectrodes in the cerebral cortex. J. Neural Eng. 2005; 2:103–113. http://dx.doi.org/10.1088/1741-2560/2/4/006. [PubMed: 16317234]

32. Lee H, Bellamkonda RV, Sun W, Levenston ME. Biomechanical analysis of silicon microelectrode-induced strain in the brain. J. Neural Eng. 2005; 2:81–89. http://dx.doi.org/10.1088/1741-2560/2/4/003. [PubMed: 16317231]

33. Degenhart AD, Eles J, Dum R, Mischel JL, Smalianchuk I, Endler B, Ashmore RC, Tyler-Kabara EC, Hatsopoulos NG, Wang W, Batista AP, Cui XT. Histological evaluation of a chronically-implanted electrocortico-graphic electrode grid in a non-human primate. J. Neural Eng. 2016; 13:046019. http://dx.doi.org/10.1088/1741-2560/13/4/046019. [PubMed: 27351722]

34. McConnell GC, Rees HD, Levey AI, Gutekunst C-A, Gross RE, Bellamkonda RV. Implanted neural electrodes cause chronic local inflammation that is correlated with local neurodegeneration. J. Neural Eng. 2009; 6:056003. http://dx.doi.org/10.1088/1741-2560/6/5/056003. [PubMed: 19700815]

35. Biran R, Martin DC, Tresco PA. Neuronal cell loss accompanies the brain tissue response to chronically implanted silicon microelectrode arrays. Exp. Neurol. 2005; 195:115–126. http://dx.doi.org/10.1016/j.expneurol.2005.04.020. [PubMed: 16045910]

36. Yoshida Kozai TD, Langhals NB, Patel PR, Deng X, Zhang H, Smith KL, Lahann J, Kotov NA, Kipke DR. Ultrasmall implantable composite micro-electrodes with bioactive surfaces for chronic neural interfaces. Nat. Mater. 2012; 11:1065–1073. http://dx.doi.org/10.1038/nmat3468. [PubMed: 23142839]

37. Kozai TDY, Marzullo TC, Hooi F, Langhals NB, Majewska AK, Brown EB, Kipke DR. Reduction of neurovascular damage resulting from microelec-trode insertion into the cerebral cortex using in vivo two-photon mapping. J. Neural Eng. 2010; 7:046011. http://dx.doi.org/10.1088/1741-2560/7/4/046011. [PubMed: 20644246]

38. Purcell EK, Seymour JP, Yandamuri S, Kipke DR. In vivo evaluation of a neural stem cell-seeded prosthesis. J. Neural Eng. 2009; 6:026005. http://dx.doi.org/10.1088/1741-2560/6/2/026005. [PubMed: 19287078]

39. Szarowski DH, Andersen MD, Retterer S, Spence AJ, Isaacson M, Craighead HG, Turner JN, Shain W. Brain responses to micro-machined silicon devices. Brain Res. 2003; 983:23–35. [(Accessed 6 June 2016)] http://www.ncbi.nlm.nih.gov/pubmed/12914963. [PubMed: 12914963]

40. Ravikumar M, Sunil S, Black J, Barkauskas DS, Haung AY, Miller RH, Selkirk SM, Capadona JR. The roles of blood-derived macrophages and resident microglia in the neuroinflammatory response to implanted intra-cortical microelectrodes. Biomaterials. 2014; 35:8049–8064. http://dx.doi.org/10.1016/j.biomaterials.2014.05.084. [PubMed: 24973296]

41. Kozai TDY, Vazquez AL, Weaver CL. In vivo two-photon microscopy reveals immediate microglial reaction to implantation of microelectrode through. J. Neural Eng. 2012; 9 http://dx.doi.org/10.1088/1741-2560/9/6/066001.

42. Kozai TDY, Li X, Bodily LM, Caparosa EM, Zenonos GA, Carlisle DL, Friedlander RM, Cui XT. Effects of caspase-1 knockout on chronic neural recording quality and longevity: insight into cellular and molecular mechanisms of the reactive tissue response. Biomaterials. 2014; 35:9620–9634. http://dx.doi.org/10.1016/j.biomaterials.2014.08.006. [PubMed: 25176060]

43. Karumbaiah L, Norman SE, Rajan NB, Anand S, Saxena T, Betancur M, Patkar R, Bellamkonda RV. The upregulation of specific interleukin (IL) receptor antagonists and paradoxical enhancement of neuronal apoptosis due to electrode induced strain and brain micromotion. Biomaterials. 2012; 33:5983–5996. http://dx.doi.org/10.1016/j.biomaterials.2012.05.021. [PubMed: 22681976]

44. Seymour JP, Kipke DR. Neural probe design for reduced tissue encapsulation in CNS. Biomaterials. 2007; 28:3594–3607. http://dx.doi.org/10.1016/j.biomaterials.2007.03.024. [PubMed: 17517431]

45. Williams JC, Hippensteel JA, Dilgen J, Shain W, Kipke DR. Complex impedance spectroscopy for monitoring tissue responses to inserted neural implants. J. Neural Eng. 2007; 4:410–423. http://dx.doi.org/10.1088/1741-2560/4/4/007. [PubMed: 18057508]

46. Kozai TDY, Eles JR, Vazquez AL, Cui XT. Two-photon imaging of chronically implanted neural electrodes: sealing methods and new insights. J. Neurosci. Methods. 2016; 258:46–55. http://dx.doi.org/10.1016/j.jneumeth.2015.10.007. [PubMed: 26526459]

47. Patel PR, Na K, Zhang H, Kozai TDY, Kotov NA, Yoon E, Chestek CA. Insertion of linear 8.4 mm diameter 16 channel carbon fiber electrode arrays for single unit recordings. J. Neural Eng. 2015; 12:046009. http://dx.doi.org/10.1088/1741-2560/12/4/046009. [PubMed: 26035638]

48. Kozai TDY, Catt K, Du Z, Na K, Srivannavit O, Haque R-UM, Seymour J, Wise KD, Yoon E, Cui XT. Chronic in vivo evaluation of PEDOT/CNT for stable neural recordings. IEEE Trans. Biomed. Eng. 2016; 63:111–119. http://dx.doi.org/10.1109/TBME.2015.2445713. [PubMed: 26087481]

49. Seymour JP, Langhals NB, Anderson DJ, Kipke DR. Novel multi-sided microelectrode arrays for implantable neural applications. Biomed. Microdevices. 2011; 13:441–451. http://dx.doi.org/10.1007/s10544-011-9512-z. [PubMed: 21301965]

50. Ludwig KA, Langhals NB, Joseph MD, Richardson-Burns SM, Hendricks JL, Kipke DR. Poly(3,4-ethylenedioxythiophene) (PEDOT) polymer coatings facilitate smaller neural recording electrodes. J. Neural Eng. 2011; 8:014001. http://dx.doi.org/10.1088/1741-2560/8/1/014001. [PubMed: 21245527]

51. Bjornsson CS, Oh SJ, Al-Kofahi YA, Lim YJ, Smith KL, Turner JN, De S, Roysam B, Shain W, Kim SJ. Effects of insertion conditions on tissue strain and vascular damage during neuroprosthetic device insertion. J. Neural Eng. 2006; 3:196–207. http://dx.doi.org/10.1088/1741-2560/3/3/002. [PubMed: 16921203]

52. Kolarcik CL, Catt K, Rost E, Albrecht IN, Bourbeau D, Du Z, Kozai TDY, Luo X, Weber DJ, Cui XT. Evaluation of poly(3,4-ethylenedioxythiophene)/ carbon nanotube neural electrode coatings for stimulation in the dorsal root ganglion. J. Neural Eng. 2015; 12:016008. http://dx.doi.org/10.1088/1741-2560/12/1/016008. [PubMed: 25485675]

53. Cui X, Wiler J, Dzaman M, Altschuler RA, Martin DC. In vivo studies of polypyrrole/peptide coated neural probes. Biomaterials. 2003; 24:777–787. [(Accessed 6 June 2016)] http://www.ncbi.nlm.nih.gov/pubmed/12485796. [PubMed: 12485796]

54. Cui X, Martin DC. Electrochemical deposition and characterization of poly(3,4-ethylenedioxythiophene) on neural microelectrode arrays. Sensors Actuators B Chem. 2003; 89:92–102. http://dx.doi.org/10.1016/S0925-4005(02)00448-3.

55. Cui X, Martin DC. Fuzzy gold electrodes for lowering impedance and improving adhesion with electrodeposited conducting polymer films. Sensors Actuators A Phys. 2003; 103:384–394. http://dx.doi.org/10.1016/S0924-4247(02)00427-2.

56. Cui X, Hetke JF, Wiler JA, Anderson DJ, Martin DC. Electrochemical deposition and characterization of conducting polymer polypyrrole/PSS on multichannel neural probes. Sensors Actuators A Phys. 2001; 93:8–18. http://dx.doi.org/10.1016/S0924-4247(01)00637-9.

57. Alba NA, Du ZJ, Catt KA, Kozai TDY, Cui XT. In vivo electrochemical analysis of a PEDOT/MWCNT neural electrode coating. Biosensors. 2007; 5:618–646. http://dx.doi.org/10.3390/bios5040618.

58. Gilgunn, PJ., Khilwani, R., Kozai, TDY., Weber, DJ., Cui, XT., Erdos, G., Ozdoganlar, OB., Fedder, GK. An ultra-compliant, scalable neural probe with molded biodissolvable delivery vehicle; 2012 IEEE 25th Int. Conf. Micro Electro Mech. Syst, IEEE. 2012. p. 56-59.http://dx.doi.org/10.1109/MEMSYS.2012.6170092

59. Zhang H, Patel PR, Xie Z, Swanson SD, Wang X, Kotov NA. Tissue-Compliant neural implants from microfabricated carbon nanotube multilayer composite. ACS Nano. 2013; 7:7619–7629. http://dx.doi.org/10.1021/nn402074y. [PubMed: 23930825]

60. Kozai TDY, Kipke DR. Insertion shuttle with carboxyl terminated self-assembled monolayer coatings for implanting flexible polymer neural probes in the brain. J. Neurosci. Methods. 2009; 184:199–205. http://dx.doi.org/10.1016/j.jneumeth.2009.08.002. [PubMed: 19666051]

61. Kolarcik CL, Luebben SD, Sapp SA, Hanner J, Snyder N, Kozai TDY, Chang E, Nabity JA, Nabity ST, Lagenaur CF, Cui XT. Elastomeric and soft conducting microwires for implantable neural

interfaces. Soft Matter. 2015; 11:4847–4861. http://dx.doi.org/10.1039/c5sm00174a. [PubMed: 25993261]

62. Harris JP, Hess AE, Rowan SJ, Weder C, Zorman CA, Tyler DJ, Capadona JR. In vivo deployment of mechanically adaptive nanocomposites for intracortical microelectrodes. J. Neural Eng. 2011; 8:046010. http://dx.doi.org/10.1088/1741-2560/8/4/046010. [PubMed: 21654037]
63. Kozai TDY, Gugel Z, Li X, Gilgunn PJ, Khilwani R, Ozdoganlar OB, Fedder GK, Weber DJ, Cui XT. Chronic tissue response to carboxymethyl cellulose based dissolvable insertion needle for ultra-small neural probes. Biomaterials. 2014; 35:9255–9268. http://dx.doi.org/10.1016/j.biomaterials.2014.07.039. [PubMed: 25128375]
64. Nesbitt KM, Varner EL, Jaquins-Gerstl A, Michael AC. Microdialysis in the rat striatum: effects of 24 h dexamethasone retrodialysis on evoked dopamine release and penetration injury. ACS Chem. Neurosci. 2015; 6:163–173. http://dx.doi.org/10.1021/cn500257x. [PubMed: 25491242]
65. Hue CD, Cho FS, Cao S, Dale Bass CR, Meaney DF, Morrison B. Dexamethasone potentiates in vitro blood-brain barrier recovery after primary blast injury by glucocorticoid receptor-mediated upregulation of ZO-1 tight junction protein. J. Cereb. Blood Flow. MetaB. 2015; 35:1191–1198. http://dx.doi.org/10.1038/jcbfm.2015.38. [PubMed: 25757751]
66. Nesbitt KM, Jaquins-Gerstl A, Skoda EM, Wipf P, Michael AC. Pharmacological mitigation of tissue damage during brain microdialysis. Anal. Chem. 2013; 85:8173–8179. http://dx.doi.org/10.1021/ac401201x. [PubMed: 23927692]
67. Luo X, Matranga C, Tan S, Alba N, Cui XT. Carbon nanotube nanoreservior for controlled release of anti-inflammatory dexamethasone. Biomaterials. 2011; 32:6316–6323. http://dx.doi.org/10.1016/j.biomaterials.2011.05.020. [PubMed: 21636128]
68. Jaquins-Gerstl A, Shu Z, Zhang J, Liu Y, Weber SG, Michael AC. Effect of dexamethasone on gliosis ischemia and dopamine extraction during microdialysis sampling in brain tissue. Anal. Chem. 2011; 83:7662–7667. http://dx.doi.org/10.1021/ac200782h. [PubMed: 21859125]
69. Leprince L, Dogimont A, Magnin D, Demoustier-Champagne S. Dexamethasone electrically controlled release from polypyrrole-coated nano-structured electrodes. J. Mater. Sci. Mater. Med. 2010; 21:925–930. http://dx.doi.org/10.1007/s10856-010-4008-6. [PubMed: 20143134]
70. Zhong Y, Bellamkonda RV. Dexamethasone-coated neural probes elicit attenuated inflammatory response and neuronal loss compared to uncoated neural probes. Brain Res. 2007; 1148:15–27. http://dx.doi.org/10.1016/j.brainres.2007.02.024. [PubMed: 17376408]
71. Wadhwa R, Lagenaur CF, Cui XT. Electrochemically controlled release of dexamethasone from conducting polymer polypyrrole coated electrode. J. Control. Release. 2006; 110:531–541. http://dx.doi.org/10.1016/j.jconrel.2005.10.027. [PubMed: 16360955]
72. Kim D-H, Martin DC. Sustained release of dexamethasone from hydrophilic matrices using PLGA nanoparticles for neural drug delivery. Biomaterials. 2006; 27:3031–3037. http://dx.doi.org/10.1016/j.biomaterials.2005.12.021. [PubMed: 16443270]
73. Spataro L, Dilgen J, Retterer S, Spence AJ, Isaacson M, Turner JN, Shain W. Dexamethasone treatment reduces astroglia responses to inserted neuro-prosthetic devices in rat neocortex. Exp. Neurol. 2005; 194:289–300. http://dx.doi.org/10.1016/j.expneurol.2004.08.037. [PubMed: 16022859]
74. Shain W, Spataro L, Dilgen J, Haverstick K, Retterer S, Isaacson M, Saltzman M, Turner JN. Controlling cellular reactive responses around neural prosthetic devices using peripheral and local intervention strategies. IEEE Trans. Neural Syst. Rehabil. Eng. 2003; 11:186–188. http://dx.doi.org/10.1109/TNSRE.2003.814800. [PubMed: 12899270]
75. Kozai TDY, Jaquins-gerstl AS, Vazquez AL, Michael AC, Cui XT. Biomaterials Dexamethasone retrodialysis attenuates microglial response to implanted probes in vivo. Biomaterials. 2016; 87:157–169. http://dx.doi.org/10.1016/j.biomaterials.2016.02.013. [PubMed: 26923363]
76. Kolarcik CL, Bourbeau D, Azemi E, Rost E, Zhang L, Lagenaur CF, Weber DJ, Cui XT. In vivo effects of L1 coating on inflammation and neuronal health at the electrode-tissue interface in rat spinal cord and dorsal root ganglion. Acta Biomater. 2012; 8:3561–3575. http://dx.doi.org/10.1016/j.actbio.2012.06.034. [PubMed: 22750248]
77. Azemi E, Lagenaur CF, Cui XT. The surface immobilization of the neural adhesion molecule L1 on neural probes and its effect on neuronal density and gliosis at the probe/tissue interface.

Biomaterials. 2011; 32:681–692. http://dx.doi.org/10.1016/j.biomaterials.2010.09.033. [PubMed: 20933270]

78. Zhong Y, Bellamkonda RV. Controlled release of anti-inflammatory agent alpha-MSH from neural implants. J. Control. Release. 2005; 106:309–318. http://dx.doi.org/10.1016/jjconrel.2005.05.012. [PubMed: 15978692]
79. Maness PF, Schachner M. Neural recognition molecules of the immunoglobulin superfamily: signaling transducers of axon guidance and neuronal migration. Nat. Neurosci. 2007; 10:19–26. http://dx.doi.org/10.1038/nn1827. [PubMed: 17189949]
80. Figge C, Loers G, Schachner M, Tilling T. Neurite outgrowth triggered by the cell adhesion molecule L1 requires activation and inactivation of the cyto-skeletal protein cofilin. Mol. Cell. Neurosci. 2012; 49:196–204. http://dx.doi.org/10.1016/j.mcn.2011.10.002. [PubMed: 22019611]
81. Lagenaur C, Lemmon V. An L1-like molecule, the 8D9 antigen, is a potent substrate for neurite extension. Proc. Natl. Acad. Sci. U. S. A. 1987; 84:7753–7757. [(Accessed 10 June 2016)] http://www.ncbi.nlm.nih.gov/pubmed/3478724. [PubMed: 3478724]
82. Lemmon V, Farr KL, Lagenaur C. L1-mediated axon outgrowth occurs via a homophilic binding mechanism. Neuron. 1989; 2:1597–1603. [(Accessed 10 June 2016)] http://www.ncbi.nlm.nih.gov/pubmed/2627381. [PubMed: 2627381]
83. Kenwrick S, Watkins A, De Angelis E. Neural cell recognition molecule L1: relating biological complexity to human disease mutations. Hum. Mol. Genet. 2000; 9:879–886. [(Accessed 10 June 2016)] http://www.ncbi.nlm.nih.gov/pubmed/10767310. [PubMed: 10767310]
84. Dihne M, Bernreuther C, Sibbe M, Paulus W, Schachner M. A new role for the cell adhesion molecule L1 in neural precursor cell proliferation, differentiation, and transmitter-specific subtype generation. J. Neurosci. 2003; 23:6638–6650. [(Accessed 10 June 2016)] http://www.ncbi.nlm.nih.gov/pubmed/12878705. [PubMed: 12878705]
85. Rathjen FG, Schachner M. Immunocytological and biochemical characterization of a new neuronal cell surface component (L1 antigen) which is involved in cell adhesion. EMBO J. 1984; 3:1–10. [(Accessed 10 June 2016)] http://www.ncbi.nlm.nih.gov/pubmed/6368220. [PubMed: 6368220]
86. Nishimune H, Bernreuther C, Carroll P, Chen S, Schachner M, Henderson CE. Neural adhesion molecules L1 and CHL1 are survival factors for motoneurons. J. Neurosci. Res. 2005; 80:593–599. http://dx.doi.org/10.1002/jnr.20517. [PubMed: 15880726]
87. Vutskits L, Djebbara-Hannas Z, Zhang H, Paccaud JP, Durbec P, Rougon G, Muller D, Kiss JZ. PSA-NCAM modulates BDNF-dependent survival and differentiation of cortical neurons. Eur. J. Neurosci. 2001; 13:1391–1402. [(Accessed 10 June 2016)] http://www.ncbi.nlm.nih.gov/pubmed/11298800. [PubMed: 11298800]
88. Hulley P, Schachner M, Lübbert H. L1 neural cell adhesion molecule is a survival factor for fetal dopaminergic neurons. J. Neurosci. Res. 1998; 53:129–134. [(Accessed 10 June 2016)] http://www.ncbi.nlm.nih.gov/pubmed/9671969. [PubMed: 9671969]
89. Takeda Y, Murakami Y, Asou H, Uyemura K. The roles of cell adhesion molecules on the formation of peripheral myelin. Keio J. Med. 2001; 50:240–248. [(Accessed 10 June 2016)] http://www.ncbi.nlm.nih.gov/pubmed/11806501. [PubMed: 11806501]
90. Aubert I, Ridet JL, Gage FH. Regeneration in the adult mammalian CNS: guided by development. Curr. Opin. Neurobiol. 1995; 5:625–635. [(Accessed 10 June 2016)] http://www.ncbi.nlm.nih.gov/pubmed/8580714. [PubMed: 8580714]
91. Xu J-C, Bernreuther C, Cui Y-F, Jakovcevski I, Hargus G, Xiao M-F, Schachner M. Transplanted L1 expressing radial glia and astrocytes enhance recovery after spinal cord injury. J. Neurotrauma. 2011; 28:1921–1937. http://dx.doi.org/10.1089/neu.2011.1783. [PubMed: 21671795]
92. Lavdas AA, Chen J, Papastefanaki F, Chen S, Schachner M, Matsas R, Thomaidou D. Schwann cells engineered to express the cell adhesion molecule L1 accelerate myelination and motor recovery after spinal cord injury. Exp. Neurol. 2010; 221:206–216. http://dx.doi.org/10.1016/j.expneurol.2009.10.024. [PubMed: 19909742]
93. Cui Y-F, Xu J-C, Hargus G, Jakovcevski I, Schachner M, Bernreuther C. Embryonic stem cell-derived L1 overexpressing neural aggregates enhance recovery after spinal cord injury in mice. PLoS One. 2011; 6:e17126. http://dx.doi.org/10.1371/journal.pone.0017126. [PubMed: 21445247]

94. Guseva D, Angelov DN, Irintchev A, Schachner M. Ablation of adhesion molecule L1 in mice favours Schwann cell proliferation and functional recovery after peripheral nerve injury. Brain. 2009; 132:2180–2195. http://dx.doi.org/10.1093/brain/awp160. [PubMed: 19541848]

95. Roonprapunt C, Huang W, Grill R, Friedlander D, Grumet M, Chen S, Schachner M, Young W. Soluble cell adhesion molecule L1-Fc promotes locomotor recovery in rats after spinal cord injury. J. Neurotrauma. 2003; 20:871–882. http://dx.doi.org/10.1089/089771503322385809. [PubMed: 14577865]

96. Chen J, Wu J, Apostolova I, Skup M, Irintchev A, Kügler S, Schachner M. Adeno-associated virus-mediated L1 expression promotes functional recovery after spinal cord injury. Brain. 2007; 130:954–969. http://dx.doi.org/10.1093/brain/awm049. [PubMed: 17438016]

97. Chen J, Bernreuther C, Dihne M, Schachner M. Cell adhesion molecule l1-transfected embryonic stem cells with enhanced survival support regrowth of corticospinal tract axons in mice after spinal cord injury. J. Neurotrauma. 2005; 22:896–906. http://dx.doi.org/10.1089/neu.2005.22.896. [PubMed: 16083356]

98. Webb K, Budko E, Neuberger TJ, Chen S, Schachner M, Tresco PA. Substrate-bound human recombinant L1 selectively promotes neuronal attachment and outgrowth in the presence of astrocytes and fibroblasts. Biomaterials. 2001; 22:1017–1028. [(Accessed 10 June 2016)] http://www.ncbi.nlm.nih.gov/pubmed/11352083. [PubMed: 11352083]

99. Azemi E, Stauffer WR, Gostock MS, Lagenaur CF, Cui XT. Surface immobilization of neural adhesion molecule L1 for improving the biocompatibility of chronic neural probes: in vitro characterization. Acta Biomater. 2008; 4:1208–1217. http://dx.doi.org/10.1016/j.actbio.2008.02.028. [PubMed: 18420473]

100. Vega L JCM, Lee MK, Jeong JH, Smith CE, Lee KY, Chung HJ, Leckband DE, Kong H. Recapitulating cell—cell adhesion using N-Cadherin biologically tethered to substrates. Biomacromolecules. 2014; 15:2172–2179. http://dx.doi.org/10.1021/bm500335w. [PubMed: 24773064]

101. Collazos-Castro JE, Hernandez-Labrado GR, Polo JL, García-Rama C. N-Cadherin- and L1-functionalised conducting polymers for synergistic stimulation and guidance of neural cell growth. Biomaterials. 2013; 34:3603–3617. http://dx.doi.org/10.1016/j.biomaterials.2013.01.097. [PubMed: 23422593]

102. Labit H, Goldar A, Guilbaud G, Douarche C, Hyrien O, Marheineke K. A simple and optimized method of producing silanized surfaces for FISH and replication mapping on combed DNA fibers. Biotechniques. 2008; 45:649–52. 654, 656–8. http://www.ncbi.nlm.nih.gov/pubmed/19238795. [PubMed: 19238795]

103. Thevenaz P, Ruttimann UE, Unser M. A pyramid approach to subpixel registration based on intensity. IEEE Trans. Image Process. 1998; 7:27–41. http://dx.doi.org/10.1109/83.650848. [PubMed: 18267377]

104. Ridler T, Calvard S. Picture thresholding using an iterative selection method. IEEE Trans. Syst. Man. Cybern. 1978; 8:630–632. http://dx.doi.org/10.1109/TSMC.1978.4310039.

105. Gilletti A, Muthuswamy J. Brain micromotion around implants in the rodent somatosensory cortex. J. Neural Eng. 2006; 3:189–195. http://dx.doi.org/10.1088/1741-2560/3/3/001. [PubMed: 16921202]

106. Saalfeld, S. Interactive Stack Rotation. 2010. http://imagej.net/Interactive_Stack_Rotation

107. He W, McConnell GC, V Bellamkonda R. Nanoscale laminin coating modulates cortical scarring response around implanted silicon microelectrode arrays. J. Neural Eng. 2006; 3:316–326. http://dx.doi.org/10.1088/1741-2560/3/4/009. [PubMed: 17124336]

108. Winslow BD, Christensen MB, Yang W-K, Solzbacher F, Tresco PA. A comparison of the tissue response to chronically implanted Parylene-C-coated and uncoated planar silicon microelectrode arrays in rat cortex. Biomaterials. 2010; 31:9163–9172. http://dx.doi.org/10.1016/j.biomaterials.2010.05.050. [PubMed: 20561678]

109. Rao L, Zhou H, Li T, Li C, Duan YY. Polyethylene glycol-containing poly-urethane hydrogel coatings for improving the biocompatibility of neural electrodes. Acta Biomater. 2012; 8:2233–2242. http://dx.doi.org/10.1016/j.actbio.2012.03.001. [PubMed: 22406507]

110. Stence N, Waite M, Dailey ME. Dynamics of microglial activation: a confocal time-lapse analysis in hippocampal slices. Glia. 2001; 33:256–266. [(Accessed 5 July 2016)] http://www.ncbi.nlm.nih.gov/pubmed/11241743. [PubMed: 11241743]
111. Nimmerjahn A, Kirchhoff F, Helmchen F. Resting microglial cells are highly dynamic surveillants of brain parenchyma in vivo. Science. 2005; 308:1314–1318. http://dx.doi.org/10.1126/science.1110647. [PubMed: 15831717]
112. Rosidi NL, Zhou J, Pattanaik S, Wang P, Jin W, Brophy M, Olbricht WL, Nishimura N, Schaffer CB. Cortical microhemorrhages cause local inflammation but do not trigger widespread dendrite degeneration. PLoS One. 2011; 6:e26612. http://dx.doi.org/10.1371/journal.pone.0026612. [PubMed: 22028924]
113. Davalos D, Grutzendler J, Yang G, V Kim J, Zuo Y, Jung S, Littman DR, Dustin ML, Gan W-B. ATP mediates rapid microglial response to local brain injury in vivo. Nat. Neurosci. 2005; 8:752–758. http://dx.doi.org/10.1038/nn1472. [PubMed: 15895084]
114. Swiatkowski P, Murugan M, Eyo UB, Wang Y, Rangaraju S, Oh SB, Wu L-J. Activation of microglial P2Y12 receptor is required for outward potassium currents in response to neuronal injury. Neuroscience. 2016; 318:22–33. http://dx.doi.org/10.1016/j.neuroscience.2016.01.008. [PubMed: 26791526]
115. Liu GJ, Nagarajah R, Banati RB, Bennett MR. Glutamate induces directed chemotaxis of microglia. Eur. J. Neurosci. 2009; 29:1108–1118. http://dx.doi.org/10.1111/j.1460-9568.2009.06659.x. [PubMed: 19302147]
116. Cho H, Hashimoto T, Wong E, Hori Y, Wood LB, Zhao L, Haigis KM, Hyman BT, Irimia D. Microfluidic chemotaxis platform for differentiating the roles of soluble and bound amyloid-β on microglial accumulation. Sci. Rep. 2013; 3:169–175. http://dx.doi.org/10.1038/srep01823.
117. Neher JJ, Neniskyte U, Hornik T, Brown GC. Inhibition of UDP/P2Y6 purinergic signaling prevents phagocytosis of viable neurons by activated microglia in vitro and in vivo. Glia. 2014; 62:1463–1475. http://dx.doi.org/10.1002/glia.22693. [PubMed: 24838858]
118. Shahlaie K, Lyeth BG, Gurkoff GG, Muizelaar JP, Berman RF. Neuro-protective effects of selective N-type VGCC blockade on stretch-injury-induced calcium dynamics in cortical neurons. J. Neurotrauma. 2010; 27:175–187. http://dx.doi.org/10.1089/neu.2009.1003. [PubMed: 19772476]
119. Ross AE, Nguyen MD, Privman E, Venton BJ. Mechanical stimulation evokes rapid increases in extracellular adenosine concentration in the pre-frontal cortex. J. Neurochem. 2014; 130:50–60. http://dx.doi.org/10.1111/jnc.12711. [PubMed: 24606335]
120. Guthrie PB, Knappenberger J, Segal M, Bennett MV, Charles AC, Kater SB. ATP released from astrocytes mediates glial calcium waves. J. Neurosci. 1999; 19:520–528. [(Accessed 5 July 2016)] http://www.ncbi.nlm.nih.gov/pubmed/9880572. [PubMed: 9880572]
121. Chang S-Y, Kim I, Marsh MP, Jang DP, Hwang S-C, Van Gompel JJ, Goerss SJ, Kimble CJ, Bennet KE, Garris PA, Blaha CD, Lee KH. Wireless fast-scan cyclic voltammetry to monitor adenosine in patients with essential tremor during deep brain stimulation. Mayo Clin. Proc. 2012; 87:760–765. http://dx.doi.org/10.1016/j.mayocp.2012.05.006. [PubMed: 22809886]
122. Bollmann L, Koser DE, Shahapure R, Gautier HOB, Holzapfel GA, Scarcelli G, Gather MC, Ulbricht E, Franze K. Microglia mechanics: immune activation alters traction forces and durotaxis. Front. Cell. Neurosci. 2015; 9:363. http://dx.doi.org/10.3389/fncel.2015.00363. [PubMed: 26441534]
123. Saxena T, Karumbaiah L, Gaupp EA, Patkar R, Patil K, Betancur M, Stanley GB, Bellamkonda RV. The impact of chronic blood-brain barrier breach on intracortical electrode function. Biomaterials. 2013; 34:4703–4713. http://dx.doi.org/10.1016/j.biomaterials.2013.03.007. [PubMed: 23562053]
124. Sawyer AJ, Kyriakides TR. Nanoparticle-based evaluation of blood-brain barrier leakage during the foreign body response. J. Neural Eng. 2013; 10:016013. http://dx.doi.org/10.1088/1741-2560/10/1/016013. [PubMed: 23337399]
125. Gingrich MB, Junge CE, Lyuboslavsky P, Traynelis SF. Potentiation of NMDA receptor function by the serine protease thrombin. J. Neurosci. 2000; 20:4582–4595. [(Accessed 5 July 2016)] http://www.ncbi.nlm.nih.gov/pubmed/10844028. [PubMed: 10844028]

126. Nadal A, Fuentes E, Pastor J, McNaughton PA. Plasma albumin is a potent trigger of calcium signals and DNA synthesis in astrocytes. Proc. Natl. Acad. Sci. U. S. A. 1995; 92:1426–1430. [(Accessed 5 July 2016)] http://www.ncbi.nlm.nih.gov/pubmed/7877995. [PubMed: 7877995]

127. Bernstein JJ, Willingham LA, Goldberg WJ. Sequestering of immunoglobulins by astrocytes after cortical lesion and homografting of fetal cortex. Int. J. Dev. Neurosci. 1993; 11:117–124. [(Accessed 5 July 2016)] http://www.ncbi.nlm.nih.gov/pubmed/8328295. [PubMed: 8328295]

128. Nicholson C, Tao L. Hindered diffusion of high molecular weight compounds in brain extracellular microenvironment measured with integrative optical imaging. Biophys. J. 1993; 65:2277–2290. http://dx.doi.org/10.1016/S0006-3495(93)81324-9. [PubMed: 7508761]

129. Hines DJ, Hines RM, Mulligan SJ, Macvicar BA. Microglia processes block the spread of damage in the brain and require functional chloride channels. Glia. 2009; 57:1610–1618. http://dx.doi.org/10.1002/glia.20874. [PubMed: 19382211]

130. Li Y, Du X-F, Liu C-S, Wen Z-L, Du J-L. Reciprocal regulation between resting microglial dynamics and neuronal activity in vivo. Dev. Cell. 2012; 23:1189–1202. http://dx.doi.org/10.1016/j.devcel.2012.10.027. [PubMed: 23201120]

131. Davalos D, Kyu Ryu J, Merlini M, Baeten KM, Le Moan N, Petersen MA, Deerinck TJ, Smirnoff DS, Bedard C, Hakozaki H, Gonias Murray S, Ling JB, Lassmann H, Degen JL, Ellisman MH, Akassoglou K, Lassmann H, Bruck W, Lucchinetti C, Marik C, Felts PA, Bauer J, Lassmann H, Smith KJ, Vos CM, Garcia AD, Doan NB, Imura T, Bush TG, Sofroniew MV, van der Valk P, Amor S, Platten M, Steinman L, Heppner FL, Ajami B, Bennett JL, Krieger C, McNagny KM, Rossi FM, Ponomarev ED, Shriver LP, Maresz K, Dittel BN, Ransohoff RM, Perry VH, Davalos D, Davalos D, Nimmerjahn A, Kirchhoff F, Helmchen F, Meyer-Luehmann M, Bartholomaus I, Wrana JL, Saederup N, Sixt M, Kermode AG, Kirk J, Plumb J, Mirakhur M, McQuaid S, Claudio L, Raine CS, Brosnan CF, Kwon EE, Prineas JW, Wakefield AJ, More LJ, Difford J, McLaughlin JE, Gay FW, Drye TJ, Dick GW, Esiri MM, Han MH, Hochmeister S, Adams RA, Flick MJ, Akassoglou K, East E, Soulika AM, Neumann H, Raghu H, Flick MJ, Feng G, Gveric D, Huizinga R, van Horssen J, Witte ME, Schreibelt G, de Vries HE, Lassmann H, Haider L, Nikic I, Dutta R, Trapp BD, Weiner HL, Frischer JM, Haynes SE, Ohsawa K, McIlvain HB, Dichmann S, Weber MS, Prod'homme T, Zamvil SS, Hickey WF, Kimura H, Madisen L, Wang D, Schachtrup C, Lassmann H, Jung S, Bugge TH, Kim JV, Bielas SL, Hao J, Miller EW, Dickinson BC, Chang CJ. Fibrinogen-induced perivascular microglial clustering is required for the development of axonal damage in neuroinflammation. Nat. Commun. 2012; 3:1227. http://dx.doi.org/10.1038/ncomms2230. [PubMed: 23187627]

132. Roth TL, Nayak D, Atanasijevic T, Koretsky AP, Latour LL, McGavern DB. Transcranial amelioration of inflammation and cell death after brain injury. Nature. 2014; 505:223–228. http://dx.doi.org/10.1038/nature12808. [PubMed: 24317693]

133. Brown GC, Neher JJ. Microglial phagocytosis of live neurons. Nat. Publ. Gr. 2014; 15 http://dx.doi.org/10.1038/nrn3710.

134. Neumann J, Sauerzweig S, Rönicke R, Gunzer F, Dinkel K, Ullrich O, Gunzer M, Reymann KG. Microglia cells protect neurons by direct engulfment of invading neutrophil granulocytes: a new mechanism of CNS immune privilege. J. Neurosci. 2008; 28:5965–5975. http://dx.doi.org/10.1523/JNEUROSCI.0060-08.2008. [PubMed: 18524901]

135. Liu Z, Condello C, Schain A, Harb R, Grutzendler J. CX3CR1 in microglia regulates brain amyloid deposition through selective protofibrillar amyloid-β phagocytosis. J. Neurosci. 2010; 30

136. Kowitz A, Kadmon G, Eckert M, Schirrmacher V, Schachner M, Altevogt P. Expression and function of the neural cell adhesion molecule L1 in mouse leukocytes. Eur. J. Immunol. 1992; 22:1199–1205. http://dx.doi.org/10.1002/eji.1830220514. [PubMed: 1577062]

137. Kadmon G, Altevogt P, The A, Sams M. The cell adhesion molecule L1: species- and cell-type-dependent multiple binding mechanisms. Differentiation. 1997; 61:143–150. [PubMed: 9084132]

138. Oleszewski M, Beer S, Katich S, Geiger C, Zeller Y, Rauch U, Altevogt P. Integrin and neurocan binding to L1 involves distinct ig domains *. J. Biol. Chem. 1999; 274:24602–24610. [PubMed: 10455125]

139. Montgomery AM, Becker JC, Siu CH, Lemmon VP, Cheresh DA, Pancook JD, Zhao X, Reisfeld RA. Human neural cell adhesion molecule L1 and rat homologue NILE are ligands for integrin

alpha v beta 3. J. Cell Biol. 1996; 132:475–485. http://dx.doi.org/10.1083/jcb.132.3.475. [PubMed: 8636223]

140. Hailer NP, Jarhult JD, Nitsch R. Resting microglial cells in vitro: analysis of morphology and adhesion molecule expression in organotypic hippocampal slice cultures. Glia. 1996; 18:319–331. [(Accessed 5 July 2016)] http://www.ncbi.nlm.nih.gov/pubmed/8972800. [PubMed: 8972800]
141. Milner R, Campbell IL. The extracellular matrix and cytokines regulate microglial integrin expression and activation. J. Immunol. 2003; 170:3850–3858. http://dx.doi.org/10.4049/jimmunol.170.7.3850. [PubMed: 12646653]
142. Nasu-Tada K, Koizumi S, Inoue K. Involvement of β1 integrin in microglial chemotaxis and proliferation on fibronectin: different regulations by ADP through PKA. Glia. 2005; 52:98–107. http://dx.doi.org/10.1002/glia.20224. [PubMed: 15920726]
143. Yip Tam W, Him Eddie Ma C. Bipolar/rod-shaped microglia are proliferating microglia with distinct M1/M2 phenotypes, (n.d.).
144. Cherry JD, Olschowka JA, O'Banion MK. Neuroinflammation and M2 microglia: the good, the bad, and the inflamed. J. Neuroinflammation. 2014; 11:98. http://dx.doi.org/10.1186/1742-2094-11-98. [PubMed: 24889886]
145. Kumar A, Stoica BA, Sabirzhanov B, Burns MP, Faden AI, Loane DJ. Traumatic brain injury in aged animals increases lesion size and chronically alters microglial/macrophage classical and alternative activation states. Neurobiol. Aging. 2013; 34:1397–1411. http://dx.doi.org/10.1016/j.neurobiolaging.2012.11.013. [PubMed: 23273602]
146. Zhang X-M, Lund H, Mia S, Parsa R, Harris RA. Adoptive transfer of cytokine-induced immunomodulatory adult microglia attenuates experimental autoimmune encephalomyelitis in DBA/1 mice. Glia. 2014; 62:804–817. http://dx.doi.org/10.1002/glia.22643. [PubMed: 24677019]
147. Peferoen LAN, Vogel DYS, Ummenthum K, Breur M, Heijnen PDAM, Gerritsen WH, Peferoen-Baert RMB, van der Valk P, Dijkstra CD, Amor S. Activation status of human microglia is dependent on lesion formation stage and remyelination in multiple sclerosis. J. Neuropathol. Exp. Neurol. 2015; 74:48–63. http://dx.doi.org/10.1097/NEN.0000000000000149. [PubMed: 25470347]
148. Durafourt BA, Moore CS, Zammit DA, Johnson TA, Zaguia F, Guiot M-C, Bar-Or A, Antel JP. Comparison of polarization properties of human adult microglia and blood-derived macrophages. Glia. 2012; 60:717–727. http://dx.doi.org/10.1002/glia.22298. [PubMed: 22290798]
149. Neher JJ, Neniskyte U, Zhao J-W, Bal-Price A, Tolkovsky AM, Brown GC. Inhibition of microglial phagocytosis is sufficient to prevent inflammatory neuronal death. J. Immunol. 2011; 186:4973–4983. http://dx.doi.org/10.4049/jimmunol.1003600. [PubMed: 21402900]
150. BalPrice A, Brown GC. Inflammatory neurodegeneration mediated by nitric oxide from activated glia-inhibiting neuronal respiration, causing glutamate release and excitotoxicity. J. Neurosci. 2001; 21:6480–6491. [(Accessed 24 October 2016)] http://www.ncbi.nlm.nih.gov/pubmed/11517237. [PubMed: 11517237]
151. Schutte RJ, Xie L, Klitzman B, Reichert WM. In vivo cytokine-associated responses to biomaterials. Biomaterials. 2009; 30:160–168. http://dx.doi.org/10.1016/j.biomaterials.2008.09.026. [PubMed: 18849070]
152. Kim D-H, Smith JT, Chilkoti A, Reichert WM. The effect of covalently immobilized rhIL-1ra-ELP fusion protein on the inflammatory profile of LPS-stimulated human monocytes. Biomaterials. 2007; 28:3369–3377. http://dx.doi.org/10.1016/j.biomaterials.2007.04.010. [PubMed: 17482260]
153. Cherry JF, Bennett NK, Schachner M, Moghe PV. Engineered N-cadherin L1 biomimetic substrates concertedly promote neuronal differentiation neurite extension and neuroprotection of human neural stem cells. Acta Biomater. 2014; 10:4113–4126. http://dx.doi.org/10.1016/j.actbio.2014.06.001. [PubMed: 24914828]
154. Barbin G, Aigrot MS, Charles P, Foucher A, Grumet M, Schachner M, Zalc B, Lubetzki C. Axonal cell-adhesion molecule L1 in CNS myelination. Neuron Glia Biol. 2004; 1:65–72. http://dx.doi.org/10.1017/S1740925×04000092. [PubMed: 18634607]

155. Akerboom J, Chen T-W, Wardill TJ, Tian L, Marvin JS, Mutlu S, Calderon NC, Esposti F, Borghuis BG, Sun XR, Gordus A, Orger MB, Portugues R, Engert F, Macklin JJ, Filosa A, Aggarwal A, Kerr RA, Takagi R, Kracun S, Shigetomi E, Khakh BS, Baier H, Lagnado L, Wang SS-H, Bargmann CI, Kimmel BE, Jayaraman V, Svoboda K, Kim DS, Schreiter ER, Looger LL. Optimization of a GCaMP calcium indicator for neural activity imaging. J. Neurosci. 2012; 32:13819–13840. http://dx.doi.org/10.1523/JNEUROSCI.2601-12.2012. [PubMed: 23035093]

156. Hoek RM, Ruuls SR, Murphy CA, Wright GJ, Goddard R, Zurawski SM, Blom B, Homola ME, Streit WJ, Brown MH, Barclay AN, Sedgwick JD. Down-regulation of the macrophage lineage through interaction with OX2 (CD200). Science. 2000; 290:1768–1771. http://dx.doi.org/10.1126/science.290.5497.1768. [PubMed: 11099416]

157. Junker A, Krumbholz M, Eisele S, Mohan H, Augstein F, Bittner R, Lassmann H, Wekerle H, Hohlfeld R, Meinl E. MicroRNA profiling of multiple sclerosis lesions identifies modulators of the regulatory protein CD47. Brain. 2009; 132:3342–3352. http://dx.doi.org/10.1093/brain/awp300. [PubMed: 19952055]

158. Harrison JK, Jiang Y, Chen S, Xia Y, Maciejewski D, McNamara RK, Streit WJ, Salafranca MN, Adhikari S, Thompson DA, Botti P, Bacon KB, Feng L. Role for neuronally derived fractalkine in mediating interactions between neurons and CX3CR1-expressing microglia. Proc. Natl. Acad. Sci. U. S. A. 1998; 95:10896–10901. [(Accessed 29 July 2016)] http://www.ncbi.nlm.nih.gov/pubmed/9724801. [PubMed: 9724801]

159. Araki T, Yamada M, Ohnishi H, Sano SI, Hatanaka H. BIT/SHPS-1 enhances brain-derived neurotrophic factor-promoted neuronal survival in cultured cerebral cortical neurons. J. Neurochem. 2000; 75:1502–1510. [(Accessed 29 July 2016)] http://www.ncbi.nlm.nih.gov/pubmed/10987830. [PubMed: 10987830]

160. Patel PR, Zhang H, Robbins M, Nofar J, Marshal S, Kobylarek M, Kozai TDY, Kotov NA, Chestek C. Chronic in vivo stability assessment of carbon fiber microelectrode arrays. J. Neural Eng. 2016; 13:066002. http://dx.doi.org/10.1088/1741-2560/13/6/066002. [PubMed: 27705958]

161. Sohal HS, Clowry GJ, Jackson A, O'Neill A, Baker SN. Mechanical flexibility reduces the foreign body response to long-term implanted microelectrodes in rabbit cortex. PLoS One, PLoS One. 2016; 11:e0165606. http://dx.doi.org/10.1371/journal.pone.0165606. [PubMed: 27788240]

162. Khilwani R, Gilgunn PJ, Kozai TDY, Ong XC, Korkmaz E, Gunalan P, Cui XT, Fedder GK, Ozdoganlar OB. Ultra-miniature ultra-compliant neural probes with dissolvable delivery needles: design, fabrication and characterization. Biomed. Microdevices. 2016; 18:97. http://dx.doi.org/10.1007/s10544-016-0125-4. [PubMed: 27778225]

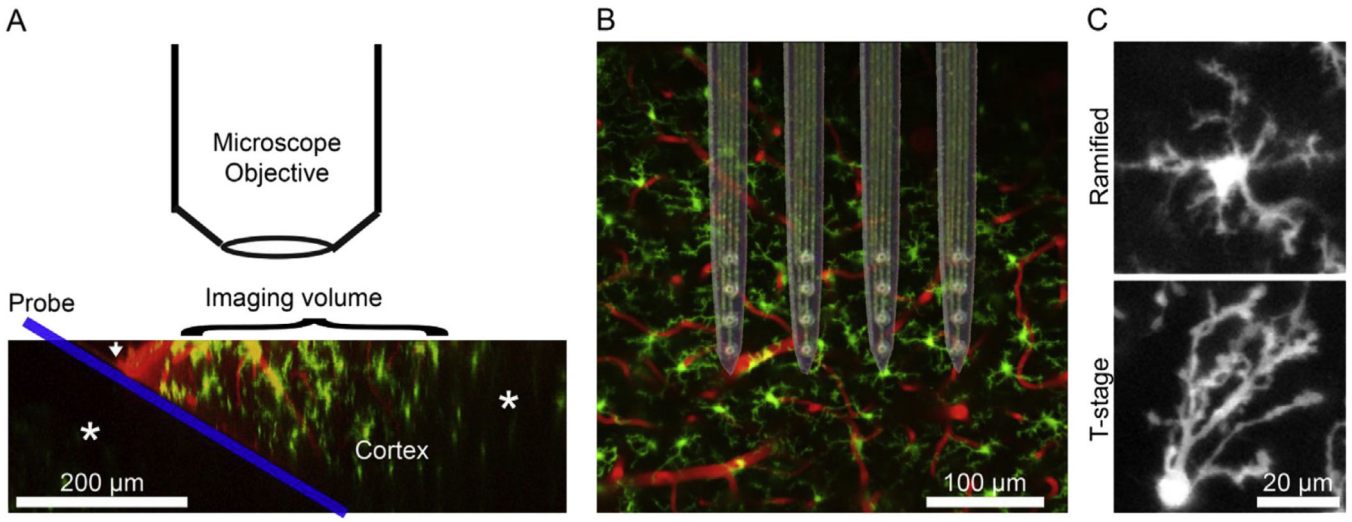

Fig. 1.

Experimental set-up. A) Following craniotomy, the probe (blue) is inserted into the cortex (Microglia in green; blood vessels in red) at a 30° angle. The white arrow indicates where the cortex is pierced. This allows the probe to be inserted without colliding with the microscope objective while maximizing the area of the probe that can be imaged. * denote darker regions due to being underneath either the probe or pial blood vessels. The image shown here is a side-projection of raw data made through a 3D reconstruction. B) Raw data were images of cortex from a "bird's-eye view". Here, a bright-field image of the neural probes is superimposed over unimplanted cortex to demonstrate probe configuration and relative of cortex and implants. The implanted probes are 4-shank, silicon Michigan-style electrodes with Ir electrode sites. C) Microglia are classified as ramified if processes extend equally in all directions or as "activated" transition stage (T-stage) if processes extend in one direction preferentially. (For interpretation of the references to colour in this figure legend, the reader is referred to the web version of this article.)

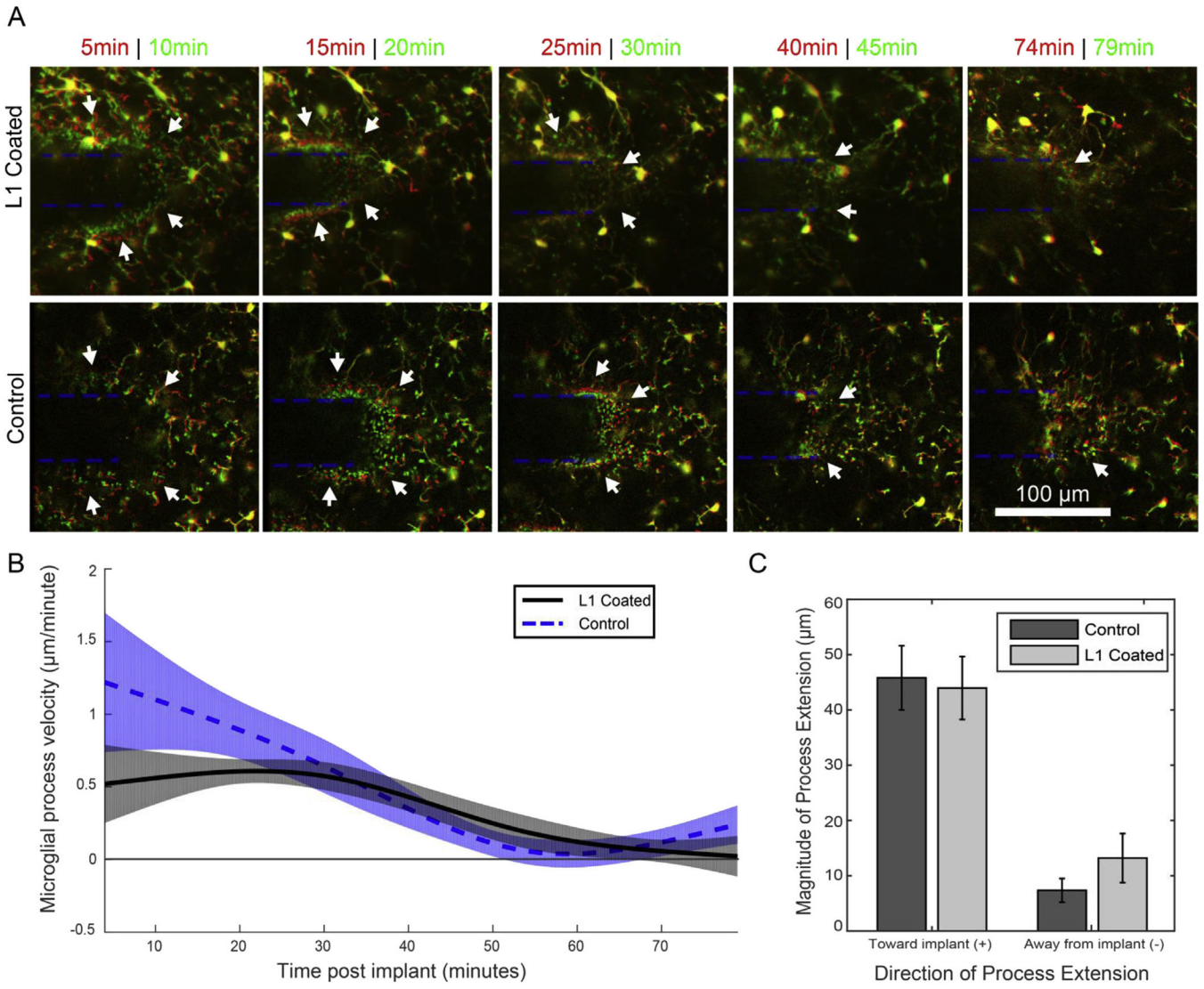

Fig. 2.

Microglial process extension velocity is unaffected by L1 coating. A) Process end-feet velocity and direction (toward (+) or away (−) from the probe, which is outlined in a blue dotted lines) are measured by comparing earlier time-point positions (red) to later (green). Yellow indicates features that did not move in that time interval. Arrows indicate the regions of advancing microglial processes, which can be identified by a layer of red processes followed by a layer of green processes. Forward progress dwindled at later time intervals (after 45 min). B) Process velocity data was modeled with a linear mixed model for the L1 group (black, solid line) and the control group (blue, dotted line). Shaded regions are 95% confidence intervals. Likelihood ratio tests revealed no group-wise differences. C) There were no significant differences in total movement toward or away from the neural probe between the L1 and control groups. Bar plot presented as mean ± SEM. (For interpretation of the references to colour in this figure legend, the reader is referred to the web version of this article.)

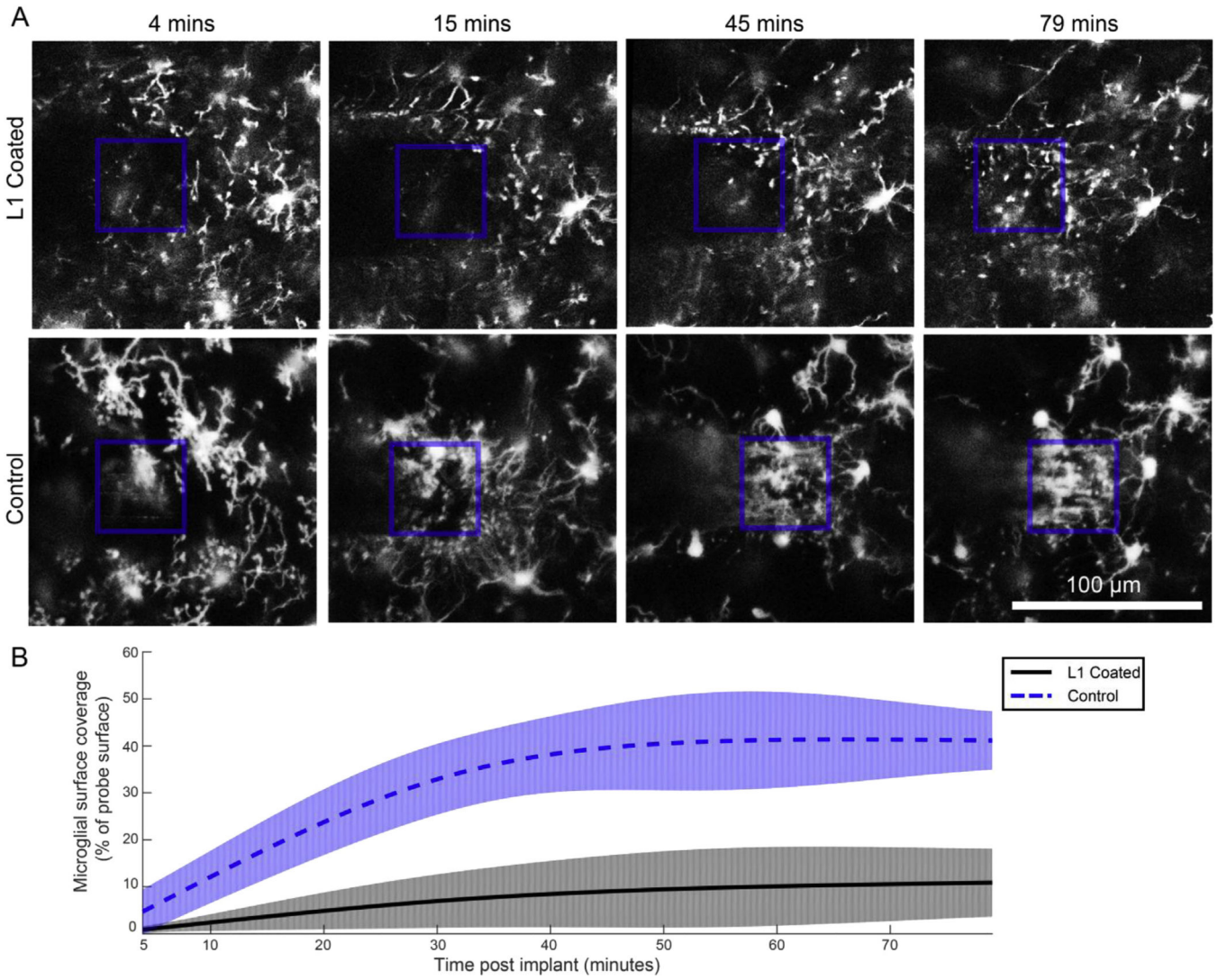

Fig. 3.

L1 prevents microglial surface coverage of neural probes over the first 79 min post-implant. A) An automated, threshold-based method quantified the percentage of probe faces covered by microglia processes. The aspect of the neural probe that was in focus is outlined in a blue box. B) Coverage data was modeled with a linear mixed model for the L1 group (black, solid line) and control group (blue, dotted line). The likelihood ratio test revealed significant group wise differences ($p < 0.01$), with 95% confidence intervals (shaded aspects of traces) diverging by 8 min post-implant. (For interpretation of the references to colour in this figure legend, the reader is referred to the web version of this article.)

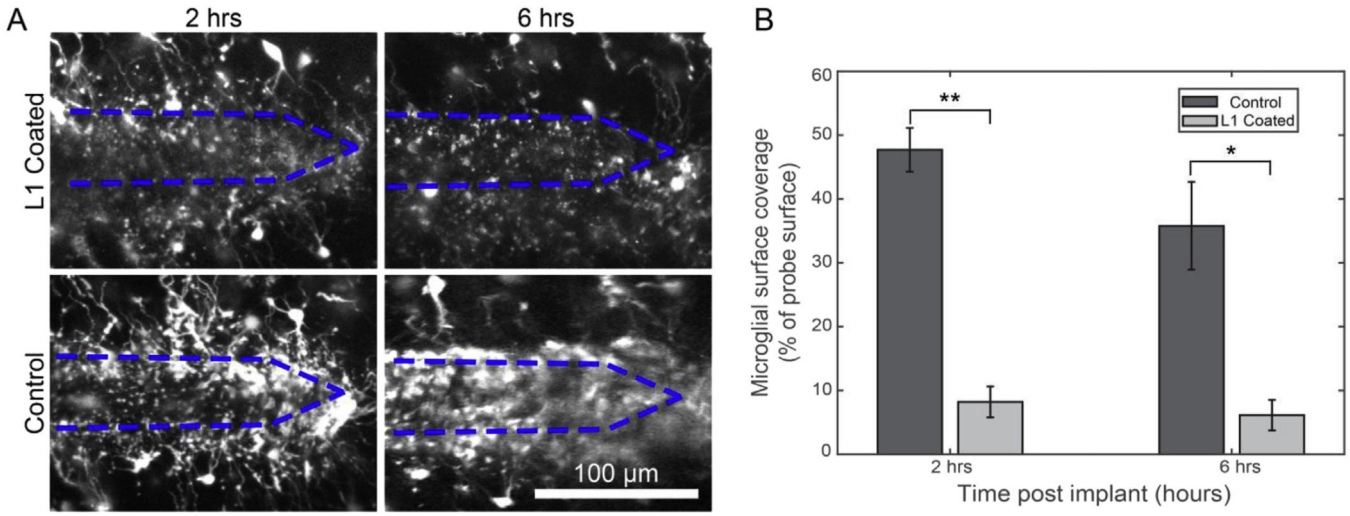

Fig. 4.

L1 coating continues to prevent microglial surface coverage through 6 h post-implant. A) 2D projections of probes at 2 and 6 h post-implant B) The percentage of the probe's surface that was covered by microglia was significantly less for L1-coated probes compared to control probes at 2 h and 6 h post-implant (Welch's T-test; $^{**}p < 0.001$, $^{*}p < 0.05$). Bar graph data presented as mean ± SEM.

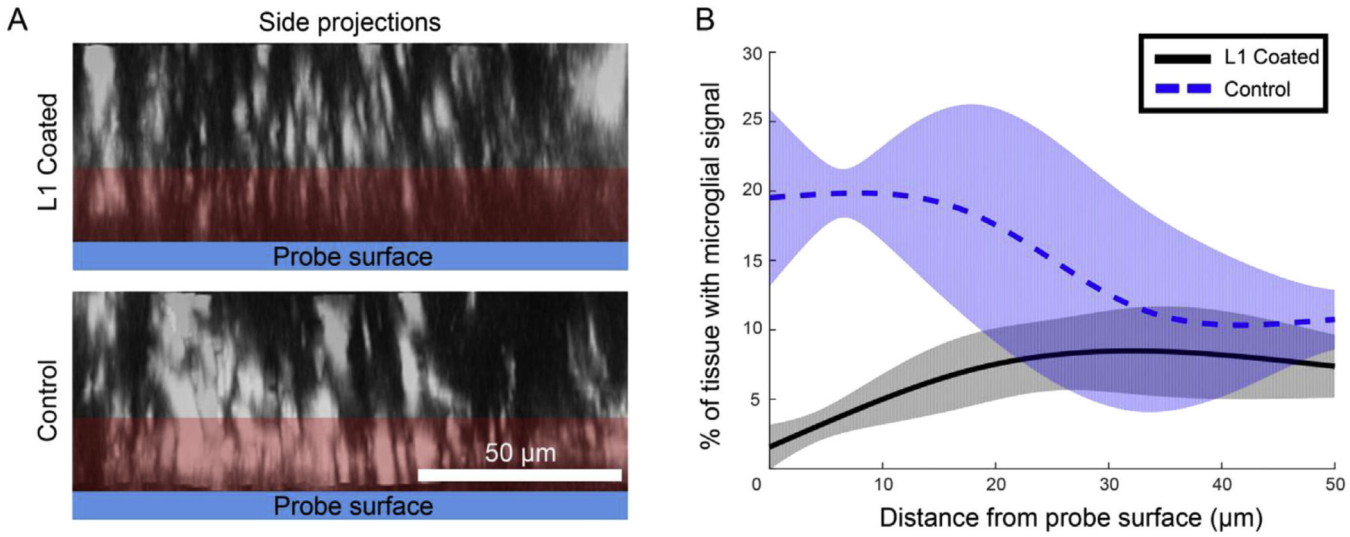

Fig. 5.

Decreases in the % of tissue with microglial signal adjacent to L1 coated probes. A) Side projections of *Z* stacks allow the microglial signal in the Z-direction above probes to be measured. The red region indicates where there are significant differences between groups. B) % of tissue with microglial signal data was modeled with a linear mixed model for the L1 group (black, solid line) and control group (blue, dotted line). The likelihood ratio test revealed significant group wise differences ($p < 0.0001$), with 95% confidence intervals (shaded aspects of traces) diverging at 20 min post-implant. (For interpretation of the references to colour in this figure legend, the reader is referred to the web version of this article.)

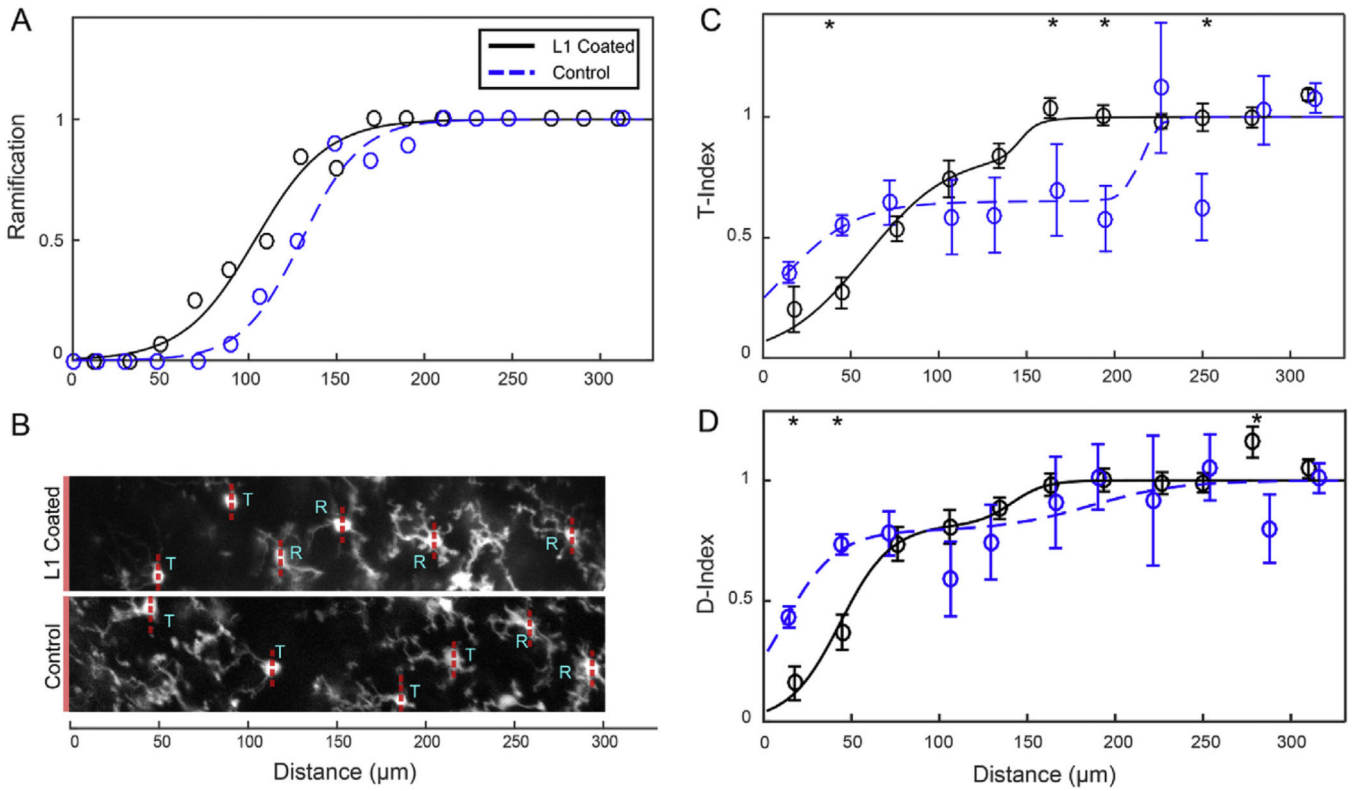

Fig. 6.

L1 coating alters morphological features at 6 h post implant. A) Probability of cell ramification (1 is ramified, 0 is T-stage) over distance show that the L1 group (black, solid line) has ramified cells closer to the probe than the control group (blue dotted line) in a logistic regression of probability data. Note: as this is a Bernolli Probability Distribution, error bars were not calculated. B) A sample image of microglia labeled as T-stage or ramified. A solid red bar at the left of each image indicates the surface of the probe. Red dotted lines indicate the axis that was used to distinguish the hemispheres facing toward the probe (left side of line) v. away from the probe (right side of line). C) The T-stage index (T-Index) compares the length of the longest probe-facing process to the longest non-probe facing process, with 0 indicating no non-probe facing processes and 1 indicating fully ramified microglia. D) The directionality index (D-Index) compares number of probe facing processes to number of non-probe facing processes, with 0 indicating all probe-facing processes and 1 indicating totally ramified microglia. Data are presented as means ± SEM; all comparisons are made by Welch's T-tests. * denotes significance, $p < 0.05$. (For interpretation of the references to colour in this figure legend, the reader is referred to the web version of this article.)